TU Delft

Delft University of Technology

Additively manufactured biodegradable porous metals

Li, Yageng; Jahr, Holger; Zhou, Jie; Zadpoor, Amir Abbas

DOI
10.1016/j.actbio.2020.08.018

Publication date
2020

Document Version
Final published version

Published in
Acta Biomaterialia

Citation (APA)
Li, Y., Jahr, H., Zhou, J., & Zadpoor, A. A. (2020). Additively manufactured biodegradable porous metals. *Acta Biomaterialia*, *115*, 29-50. https://doi.org/10.1016/j.actbio.2020.08.018

Important note
To cite this publication, please use the final published version (if applicable).
Please check the document version above.

Copyright
Other than for strictly personal use, it is not permitted to download, forward or distribute the text or part of it, without the consent of the author(s) and/or copyright holder(s), unless the work is under an open content license such as Creative Commons.

Takedown policy
Please contact us and provide details if you believe this document breaches copyrights.
We will remove access to the work immediately and investigate your claim.

This work is downloaded from Delft University of Technology.
For technical reasons the number of authors shown on this cover page is limited to a maximum of 10.

Acta Biomaterialia 115 (2020) 29–50

Contents lists available at ScienceDirect

Acta Biomaterialia

journal homepage: www.elsevier.com/locate/actbio

Review paper

Additively manufactured biodegradable porous metals

Yageng Li[a,*], Holger Jahr[b,c], Jie Zhou[a,1], Amir Abbas Zadpoor[a,1]

[a] Department of Biomechanical Engineering, Delft University of Technology, Delft 2628 CD, Netherlands
[b] Department of Anatomy and Cell Biology, University Hospital RWTH Aachen, Aachen 52074, Germany
[c] Department of Orthopedic Surgery, Maastricht UMC+, Maastricht 6202 AZ, Netherlands

ARTICLE INFO

Article history:
Received 19 June 2020
Revised 27 July 2020
Accepted 13 August 2020
Available online 25 August 2020

Keywords:
Additive manufacturing
Metal
Scaffold
Biodegradation
Mechanical property
Biocompatibility

ABSTRACT

Partially due to the unavailability of ideal bone substitutes, the treatment of large bony defects remains one of the most important challenges of orthopedic surgery. Additively manufactured (AM) biodegradable porous metals that have emerged since 2018 provide unprecedented opportunities for fulfilling the requirements of an ideal bone implant. First, the multi-scale geometry of these implants can be customized to mimic the human bone in terms of both micro-architecture and mechanical properties. Second, a porous structure with interconnected pores possesses a large surface area, which is favorable for the adhesion and proliferation of cells and, thus, bony ingrowth. Finally, the freeform geometrical design of such biomaterials could be exploited to adjust their biodegradation behavior so as to maintain the structural integrity of the implant during the healing process while ensuring that the implant disappears afterwards, paving the way for full bone regeneration. While the AM biodegradable porous metals that have been studied so far have shown many unique properties as compared to their solid counterparts, the unprecedented degree of flexibility in their geometrical design has not yet been fully exploited to optimize their properties and performance. In order to develop the ideal bone implants, it is important to take advantage of the full potential of AM biodegradable porous metals through detailed and systematic study on their biodegradation behavior, mechanical properties, biocompatibility, and bone regeneration performance. This review paper presents the state of the art in AM biodegradable porous metals and is focused on the effects of material type, processing, geometrical design, and post-AM treatments on the mechanical properties, biodegradation behavior, *in vitro* biocompatibility, and *in vivo* bone regeneration performance of AM porous Mg, Fe, and Zn as well as their alloys. We also identify a number of knowledge gaps and the challenges encountered in adopting AM biodegradable porous metals for orthopedic applications and suggest some promising areas for future research.

© 2020 Acta Materialia Inc. Published by Elsevier Ltd.
This is an open access article under the CC BY-NC-ND license
(http://creativecommons.org/licenses/by-nc-nd/4.0/)

1. Introduction

1.1. Background

The world is experiencing a rapidly increasing demand for bone implants due to an expanding and aging population, which increases both the rate and number of such incidents as trauma, bony tumors, and skeletal deformities [1]. Implants for the treatment of critical-sized bony defects are particularly sought after, as such defects seriously affect the quality and length of patients' lives [2]. However, as of today, the treatment of large bony defects remains one of the primary challenges of orthopedic surgery. Although bone is known to have self-healing abilities, large bony defects cannot heal by themselves, if left untreated. Interventions, such as bone-grafting are, therefore, necessary to restore the bony tissue [3]. Every year, more than two million bone-grafting operations are performed all over the world [4]. The clinically applied bone grafts include autografts (bone taken from the same person's body), allografts (bone tissue from a deceased donor), and xenografts (bone tissue from an animal). Among those, autografts are superior because of their lower risks of eliciting foreign body response and transmitting diseases while offering improved osteogenesis [5]. However, even autografts suffer from major limitations of which limited supply, the need for multiple (lengthy) operations, and donor-site morbidity are the most prominent ones [6]. To address those limitations, the concept of synthetic bone substitutes has emerged. Apart from being biocompatible, an ideal bone

* Corresponding author:
E-mail address: y.li-7@tudelft.nl (Y. Li).
[1] Authors contributed equally to the study.

https://doi.org/10.1016/j.actbio.2020.08.018
1742-7061/© 2020 Acta Materialia Inc. Published by Elsevier Ltd. This is an open access article under the CC BY-NC-ND license
(http://creativecommons.org/licenses/by-nc-nd/4.0/)

substitute offers mechanical properties close to those of the native bone in order to provide sufficient mechanical support on the one hand and to avoid stress shielding on the other [7], present a fully-interconnected porous structure to allow for bony ingrowth [8,9], and degrade in the human body at an appropriate rate as the bone regenerates [10]. However, it has been so far challenging to develop a porous biomaterial that can fulfill all these requirements. The quest for an ideal bone substituting material is, therefore, still at full swing [11].

1.2. Choice of materials

A variety of bone-substituting porous biomaterials based on polymers, ceramics, and metals have been developed in recent years [12]. Among the three categories of biomaterials, polymer-based biomaterials have great design flexibility for tailored biodegradation behavior and offer a multitude of routes to biofunctionalization [13]. Ceramic-based biomaterials are, on the other hand, well known for their favorable biodegradability and superior osteoconductivity [14]. The main drawback of polymer-based biomaterials is their low mechanical properties, while ceramic-based biomaterials are brittle in nature [4]. On the contrary, metallic porous biomaterials, because of their remarkable strength and significant energy absorption capacity, are considered to be the most suitable candidates for load-bearing orthopedic implants [15]. Traditional metallic biomaterials are made from metals with high corrosion resistance. Therefore, they permanently remain in the human body, impeding full bone tissue regeneration and creating the risk of implant-associated infection due to the colonization of their surface by biofilm-forming bacteria [16]. Bio-inert implants may also cause long-term endothelial dysfunction, permanent physical irritation, and chronic inflammatory local reactions [17]. Metallic biomaterials with proper biodegradability are, therefore, of great potential utility for orthopedic and trauma surgeries. It is, of course, important to carefully design and analyze such biodegradable metallic biomaterials to make sure they only release biodegradation products that are biocompatible and can be metabolized by the human body. Consequently, the major elements constituting a biodegradable metal are often the essential trace elements that naturally occur in the body. To date, magnesium, iron, and zinc as well as their alloys have been considered to be the most appropriate candidates [18].

1.3. Geometrical design

It is well known that the human bone has a highly hierarchical structure at different length scales, including macroscale, microscale, sub-microscale, nanoscale, and sub-nanoscale (Fig. 1a) [19]. At the macroscale level, bone can be classified as being either cortical or trabecular with varied porosities and mechanical properties. To better mimic the mechanical properties and functionalities of the human bone, ideal bone substitutes need to possess bone-mimicking geometries. Moreover, an appropriate design of a porous metallic biomaterial requires careful selection of pore shape, pore size, and porosity. Those characteristics can not only affect the mechanical properties of porous metallic biomaterials [20] but can also significantly influence their biological performance, such as cell adhesion and proliferation, nutrient transportation, and bone ingrowth [9,21].

1.4. Fabrication

To realize the complex geometrical designs that are deemed necessary for an ideal bone substitute, much effort has been spent on developing biodegradable porous metals through casting, sintering, foaming, and chemical vapor deposition [22–56]. However, such conventional techniques can neither precisely control the geometry nor achieve the appropriate level of mechanical properties [57]. The advent of and recent progress in additive manufacturing (AM) technique has provided an unprecedented opportunity to tackle the dilemma of free-form design and manufacturing feasibility encountered in fabricating an ideal porous metallic biomaterial. Up until now, three main types of metal AM techniques, namely directed energy deposition (DED), powder bed fusion (PBF), and binder jetting (BJ) have been applied to the fabrication of AM porous implants (Fig. 1b-e) [58]. DED and PBF are considered to be direct AM metal printing techniques, while BJ needs post-AM treatment, typically debinding and sintering. According to the heat source (*i.e.*, laser (L) or electron beam (EB)), DED and PBF can be further categorized as DED-L (Fig. 1b), DED-EB (Fig. 1c), selective laser melting (SLM) (Fig. 1d), and electron beam melting (EBM) (Fig. 1e). While DED is mostly used for the fabrication of large rough parts, PBF is considered to be the most appropriate method for building complex porous structures [58], typical of metallic implants.

A large number of AM bio-inert metallic materials have been investigated, such as titanium [59] and its alloys [60–62], stainless steel [63], tantalum [64], and cobalt-chromium [65]. A combination of a high level of interconnected porosity and bone-mimicking mechanical properties has been achieved for several of those biomaterials [62,64]. However, as mentioned in SubSection 1.2, those biomaterials do not biodegrade over time, meaning that bone regeneration cannot be completed. Only AM biodegradable porous metals have the great potential to meet all the requirements for ideal bone implants. However, unlike AM bio-inert titanium or cobalt-chromium, AM biodegradable metals particularly Mg and Zn have low boiling temperatures and high chemical activities, which pose a set of new challenges in fabrication using the PBF processes [57]. The challenges include both those associated with the safety of the manufacturing processes, particularly in the case of Mg, and those pertaining to the quality of the resulting biomaterials. Under sub-optimal processing conditions, defects, such as voids, lack of fusion, rough surface, severe residual stresses, and distortions may occur. Even for Fe, evaporation has been found to play an important role in densification during laser melting [66]. Precise process planning and control are, therefore, required for the successful application of AM techniques for the fabrication of geometrically-ordered biodegradable porous implants.

1.5. Objective and focus

Since there have already been several papers reviewing the AM of biodegradable metals mainly from the materials processing viewpoint [67,68], the present review paper focuses on the mechanical properties, biodegradation behavior, cell responses, and *in vivo* performance of such biomaterials with an emphasis on the effects of the material type, chemical composition, processing, geometrical design, and post-AM treatments on the overall performance of AM biodegradable porous metals. We will also identify the relevant gaps in the available knowledge and the challenges encountered in adopting AM biodegradable porous metals for orthopedic applications.

2. Mechanical properties

AM biodegradable porous metallic bone implants need to provide sufficient mechanical support during the bone healing process, which is often taken to mean that they should exhibit bone-mimicking mechanical properties. The mechanical properties of

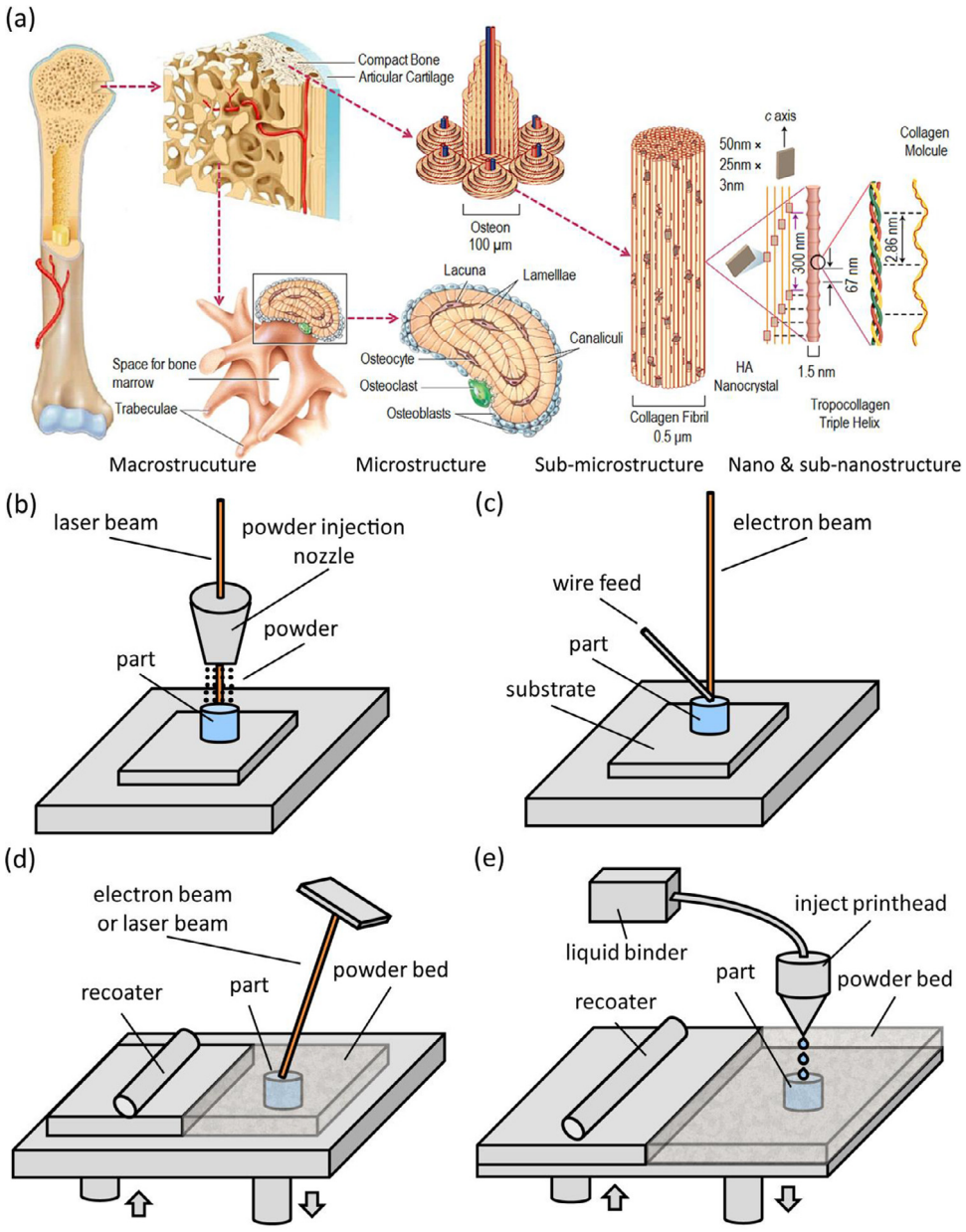

Fig. 1. The hierarchical structure of the human bone [19] (a) and schematic illustrations of the AM processes relevant for the fabrication of AM biodegradable porous metals including (b) DED-L, (c) DED-EB, (d) PBF (SLM or EBM), and (e) binder jetting.

trabecular bone (*e.g.*, yield strength and stiffness) differ greatly from those of the human cortical bone. The trabecular bone has a compressive yield strength in the range of 2–12 MPa and an elastic modulus value between 0.1 and 5 GPa, while the cortical bone has a compressive yield strength between 170 and 193 MPa and an elastic modulus value that may be as high as 20 GPa [3]. In addition, the mechanical properties of AM biodegradable porous metals must be retained at a level high enough to provide mechanical support for 12–24 weeks [69], as biodegradation takes its course. In addition to quasi-static mechanical properties, the fatigue behavior of AM biodegradable porous metals is of particular importance, as load-bearing orthopedic implants experience millions of loading cycles per year [62]. Corrosion fatigue behavior is especially relevant to biodegradable metals, as biodegradation tends to shorten their fatigue life [70]. Here we review the mechanical properties of AM biodegradable porous and bulk metals (Table 1) and discuss the effects of various relevant factors.

2.1. Material type and alloying

Among biodegradable pure metals, AM pure iron has the highest yield strength and elastic modulus (200–352 MPa and 188–215 GPa, respectively) [71–73]. These values are much higher than those of the human cortical bone, leaving ample space for introducing porosity to AM pure iron. AM pure magnesium has a similar elastic modulus value (27–35 GPa) [74,75] to the human cortical bone, but a lower yield strength (51 MPa) [76]. Since introducing porosity decreases both elastic modulus and strength, it is sensible to develop AM bulk magnesium for cortical bone fixation and AM porous magnesium for trabecular bone substitution. Conventionally manufactured pure zinc has an elastic modulus (70–140 GPa) [77], which is higher than that of the human cortical bone. The elastic modulus (12–32 GPa) [78,79] of AM pure zinc is, however, much lower than that of the traditionally manufactured pure zinc, partly due to the presence of defects even when state-of-the-art AM tech-

Table 1
The mechanical properties of AM biodegradable metals.

Material	Composition	Fabrication method	Porosity %	Unit cell	Testing method	Yield strength MPa	Elastic modulus GPa	Ultimate strength MPa	Elongation %	Hardness HV	Ref.
cortical			3-5		tensile	124–174 (L*) 53 (T)	7–19 (L) 10-11 (T) 20-27 (R)		1-3	390–770 MPa (40-79 HV)	[3] [19]
					compression	170–193 (L) 131 (T)					[39]
					bending	160					
					shear	54-65					
trabecular			up to 90			2-12	0.1-5				
Mg	pure	SLM			indentation		27-33			590–950 MPa	[74]
	pure	SLM			indentation		33-35			770 ± 80 MPa	[75]
	AZ91D	SLM			tensile	254		296	2	85-100	[90]
	WE43	SLM			tensile	296 ± 3	46 ± 2	308	12		[81]
	Mg	SLM			compression	51				38	[76]
	Mg1Sn					62				49	
	Mg3Sn					76				55	
	Mg5Sn					81				63	
	Mg7Sn					75				66	
	Mg-Zn-Zr	Binderless 3DP			compression		22	260 ± 6			[169]
					tensile			71 ± 1	0.7± 0.1		
	ZK60				compression	132 ± 4				81 ± 2	[139]
	ZK60-0.2Cu					144				88	
	ZK60-0.4Cu					158 ± 5				95	
	ZK60-0.6Cu					155				101	
	ZK60-0.8Cu					148				105 ± 3	
	CNTs/AZ31B				tensile	245		286 ± 13		94 ± 5	[170]
	AZ31				compression	377 ± 29				64 to 71	[171]
					tensile	183 ± 8		212 ± 34	8 ± 3		
	Mg-1Zn	SLM			tensile	148			11	50	[172]
	Mg-2Zn					71			2	46	
	Mg-4Zn					60			3	58	
	Mg-6Zn					45			1	65	
	Mg-8Zn					44			2	78	
	Mg-10Zn					63			2	76	
	Mg-12Zn					74			3	80	
Fe	pure	SLM			tensile	305 ± 20	215 ± 20	412 ± 25	10		[72]
	pure	SLM			tensile	256 ± 17	208 ± 16	357 ± 22	9	128-155	[71]
		SLM+anneal				352 ± 21	188 ± 10	401 ± 23	15	168-190	
	pure	SLM			compression	200				157	[73]
	Fe-2Pd-2.5bredigite	SLM			compression	161 ± 7				125	[138]
	Fe-2Pd-5bredigite				compression	147				130	
	Fe-2Pd-10bredigite					137				115	
	Fe-4Pd-2.5bredigite					175				132	
	Fe-4Pd-5bredigite					164				140	
	Fe-4Pd-10bredigite					163				120	
Zn	pure	SLM			tensile	108-122	14-32	132-138	8-12	42	[78]
	pure	SLM			tensile	122 ± 3	20 ± 6	138 ± 2	8 ± 1	46 ± 2	[114]
	pure	SLM			compression	99±22					[73]

(*continued on next page*)

Table 1 (*continued*)

Material	Composition	Fabrication method	Porosity %	Unit cell	Testing method	Yield strength MPa	Elastic modulus GPa	Ultimate strength MPa	Elongation %	Hardness HV	Ref.
	pure	SLM			tensile	93-110		117-133	3-8		[92]
	pure	SLM			compression	146				37	[80]
	Zn-2Ag					200				55	
	Zn-4Ag					217				80	
	Zn-6Ag					293				81	
	Zn-8Ag					267				79	
	Zn	SLM			tensile	43 ± 3	12 ± 2	61 ± 5	1.7 ± 0.1	50 ± 6	[79]
	Zn-1Mg					74 ± 4	19	126 ± 4	3.6 ± 0.2	93 ± 8	
	Zn-2Mg	SLM			tensile	117 ± 5	25	162 ± 6	4.1 ± 0.2	138 ± 7	
	Zn-3Mg					152 ± 5	48 ± 4	222 ± 8	7.2 ± 0.4	177 ± 9	
	Zn-4Mg					132 ± 8	58 ± 5	166 ± 7	3.1 ± 0.3	199 ± 10	
	Zn-2Al					121-171		142-192	10-12	57-65	
porous Mg	WE43	SLM	76	lattice	compression			15			[116]
	WE43+PEO		70					31			
	WE43+PEO		76					23			
	WE43+PEO+HT		76					13			
	WE43+21d							collapse			
	WE43+PEO+21d							21			
	WE43+PEO+21d							5			
	WE43+PEO+HT+21d							1			
	WE43	SLM			bending			20-23			[173]
	WE43	SLM	67	diamond	compression	23	0.8	27			[95]
	WE43 + 28d					14	0.8	14			
	Mg-5.9Zn-0.13Zr	Binderless 3DP	27		compression	40 ± 1	18.4 ± 0.1	174 ± 3			[174]
porous Fe	Fe	SLM	67 ± 2	cubic	compression	70 ± 4		135 ± 5			[85]
	Fe-25Mn			sheet	compression	137 ± 8		222 ± 11			
	Fe-35Mn	SLM	42			89 ± 2	34 ± 2	304 ± 7			[84]
	Fe	SLM	85	diamond	compression	11	1				[99]
			70			29	1				
			70			31	2				
			59			54	3				
	Fe+28d					8	1				
						26	1				
						24	1				
						48	2				
	Fe	SLM	73	diamond	compression	24	2				[93]
	Fe+28d					22	2				
	Fe	binder extrusion	66	mesh	compression	141	1				[118]
	Fe+HA					110	1				
	Fe30Mn	inkjet 3DP	36		tensile	106 ± 8	32 ± 5	116 ± 1	0.7 ± 0.2		[96]
	Fe-Mn	Binder-jetting 3DP	39 ± 2		tensile	228 ± 11	39 ± 1	190 ± 26			[97]
	Fe-Mn-1Ca		53 ± 1			297 ± 46	16 ± 21				
porous Zn	Zn	SLM	73 ± 2	diamond	compression	4	0.4				[100]
			69 ± 2			6	0.5				
			62 ± 3	diamond		11	0.8				
	Zn+28d+d					7	0.3				
						10	0.5				
						14	0.9				
	Zn+28d+s					6	0.3				
						8	0.5				
						12	0.8				
	Zn	3DP+casting	20	mesh	compression	11	0.2				[175]
			60			6	0.1				

*L, T, and R represent longitudinal, transverse, and random.

nologies are applied. Moreover, the yield strength of AM pure zinc is relatively low (43–150 MPa) [73,78–80], limiting its application for cortical bone substitution.

Alloying can be used to adjust the mechanical properties of AM biodegradable porous metals for orthopedic applications. Although the elastic modulus of Mg-based alloys is relatively insensitive to their chemical compositions [10], the yield strength can be significantly improved through appropriate alloying. SLM bulk WE43 magnesium alloy reaches a yield strength of 296.3 ± 2.5 MPa [81], which is comparable to the human cortical bone. As for zinc, alloying seems to be able to tune its stiffness and yield strength simultaneously. For instance, an SLM Zn-Mg alloy has been found to possess significantly increased elastic modulus and yield strength as compared to the pure zinc counterpart [79]. Interestingly, the addition of aluminum to zinc has been found to decrease the stiffness but increase the yield strength [82]. However, the addition of aluminum limits the biomedical applications of the alloy given the cytotoxicity of this element. Recently, Yang et al. [83] have found that Li and Mg in extruded zinc play a more effective strengthening role, as compared with other alloying elements with increased biocompatibility. Similarly, an SLM Fe-Mn alloy has shown a significantly higher yield strength than SLM pure iron [84,85].

The fatigue behavior of AM porous metal is largely dependent on the type of materials. With a similar geometrical design, AM porous pure iron and zinc have been found to show higher fatigue strengths than an AM porous magnesium alloy (WE43) [86–88]. Remarkably, AM pure iron and zinc did not show a catastrophic failure similar to the AM porous WE43 magnesium alloy during their fatigue tests (Fig. 2a), which was attributed to the highly ductile mechanical behavior of pure iron and zinc.

2.2. AM processing

The mechanical properties of porous metals are largely determined by the specific PBF process applied during their fabrication. Internal pores, inclusions, and cracks inside the struts of a scaffold can deteriorate the mechanical properties of AM porous metals (Fig. 2b) [67]. As discussed in SubSection 2.1, the elastic modulus of AM zinc is much lower than its conventionally manufactured counterparts, with the manufacturing defects accounting for the differences. The manufacturing defects in AM zinc can act as crack initiation sites, shortening its fatigue life [89]. As observed in the case of SLM AZ91 [90], optimizing the energy density can improve the densification process during SLM, thereby enhancing the mechanical properties of the resulting material.

Different SLM process parameters lead to different grain sizes and grain orientations (Fig. 2c), both of which can affect the mechanical properties of AM porous metals [91,92]. SLM biodegradable porous metals normally have much finer grain sizes than the conventionally manufactured counterparts, which can improve the strengths of those materials according to the Hall-Patch relationship [93–95]. Moreover, the different types of AM processes lead to very different mechanical properties even when the base material is the same. For instance, BJ or extrusion often results in the presence of internal pores. A post-AM treatment, such as sintering is, therefore, needed for material consolidation [96–98]. Without applying hot isostatic pressing (HIP), it is even more challenging to produce a fully densified part via sintering, as compared with PBF.

2.3. Geometrical design

Unlike AM bulk materials, the mechanical properties of porous materials are strongly dependent on their geometrical design, including their porosity and unit cell type. Similar to AM bio-inert porous metals, the yield strength and elastic modulus of AM biodegradable porous metals are directly related to their relative densities [99,100]. As for the unit cell types, there are two major types of designs, namely beam-based (*e.g.*, cubic, diamond, and dodecahedron) and sheet-based (*e.g.*, minimal surface designs including gyroid, Schwartz P (primitive), and Schwartz D (diamond) [101]). The structures designed using beam-like elements can be further divided into bending-dominated and stretch-dominated structures. Normally, a bending-dominated structure has a higher energy absorption ability, while a stretch-dominated structure has a higher stiffness and yield strength [20,102]. For example, SLM porous iron based on the cubic unit cell has been found to have a higher yield strength than that based on the diamond unit cell [85,93]. Lietaert et al. [103] compared the mechanical properties of AM porous zinc based on the diamond, dodecahedron, FCC, Kagome, and octet truss unit cells. Among those, the scaffolds based on the Kagome unit cell showed the highest yield strength for the same value of the relative density. Surprisingly, however, the strength of the scaffolds based on the octet truss cells (a stretch-dominated structure) were found to be the lowest, which was explained by the lower manufacturing quality of the octet truss scaffolds with strong particle attachment and dross formation on the horizontal struts. All the beams of a bending-dominated unit cell like the diamond unit cells are tilted at around 35° relative to the building direction. However, stretch-dominated lattice structures usually have at least some struts whose orientation is perpendicular to the building direction, reducing the manufacturing quality of those structures [104]. Furthermore, the unit cell type not only determines the mechanical properties of AM porous metals but also decides the failure mode of the scaffolds under compression. It has been shown that the abrupt diagonal shear of SLM Ti-6Al-4 V lattice can be changed to progressive layer deformation or barreling depending on the unit cell type [62,105].

All types of the human bones (*i.e.*, long, short, flat, or irregular) show a gradual change in their porosity from a compact outer cortical shell towards the spongy inner cancellous tissue. Long bones (*e.g.*, femoral head and neck region or distal radius) are some typical examples of bone structures with porosity and directionality, both highly graded and dependent on the local values of the mechanical stimuli (*e.g.*, strain energy density) [106–110]. It is, therefore, imperative that AM porous biomaterials should mimic the natural gradual structures of the human bones, particularly given the fact that they will be eventually surrounded by pockets of bony tissue with graded micro-architectures [111] and biomechanical performance [112]. Li et al. [99,100] have shown that AM functionally graded porous iron and zinc with precisely controlled geometries could be successfully fabricated by using SLM and achieve mechanical properties that are comparable with those of the human trabecular bone (Fig. 2e).

The geometrical design has also been shown to influence the fatigue behavior of AM porous biodegradable implants. For example, for the diamond unit cell, fatigue cracks tend to initiate at the junctions between the two struts where tensile stress concentration occurs under compression [86–88]. Once more, functionally graded designs could play an important role in improving the mechanical performance of AM porous biodegradable implants. For example, Li et al. [87] found that graded structural designs could increase the fatigue strength of SLM porous zinc. Similar results have been obtained for EBM functionally graded porous Ti-6Al-4 V [113]. There is currently limited data available regarding the fatigue behavior of stretch-dominated AM biodegradable lattice structures as well as that of sheet-based structures, such as those based on minimal surfaces.

2.4. Post-AM treatments

All as-built AM biodegradable porous metals have powder particles adhering to their surface. Chemical etching or sandblasting

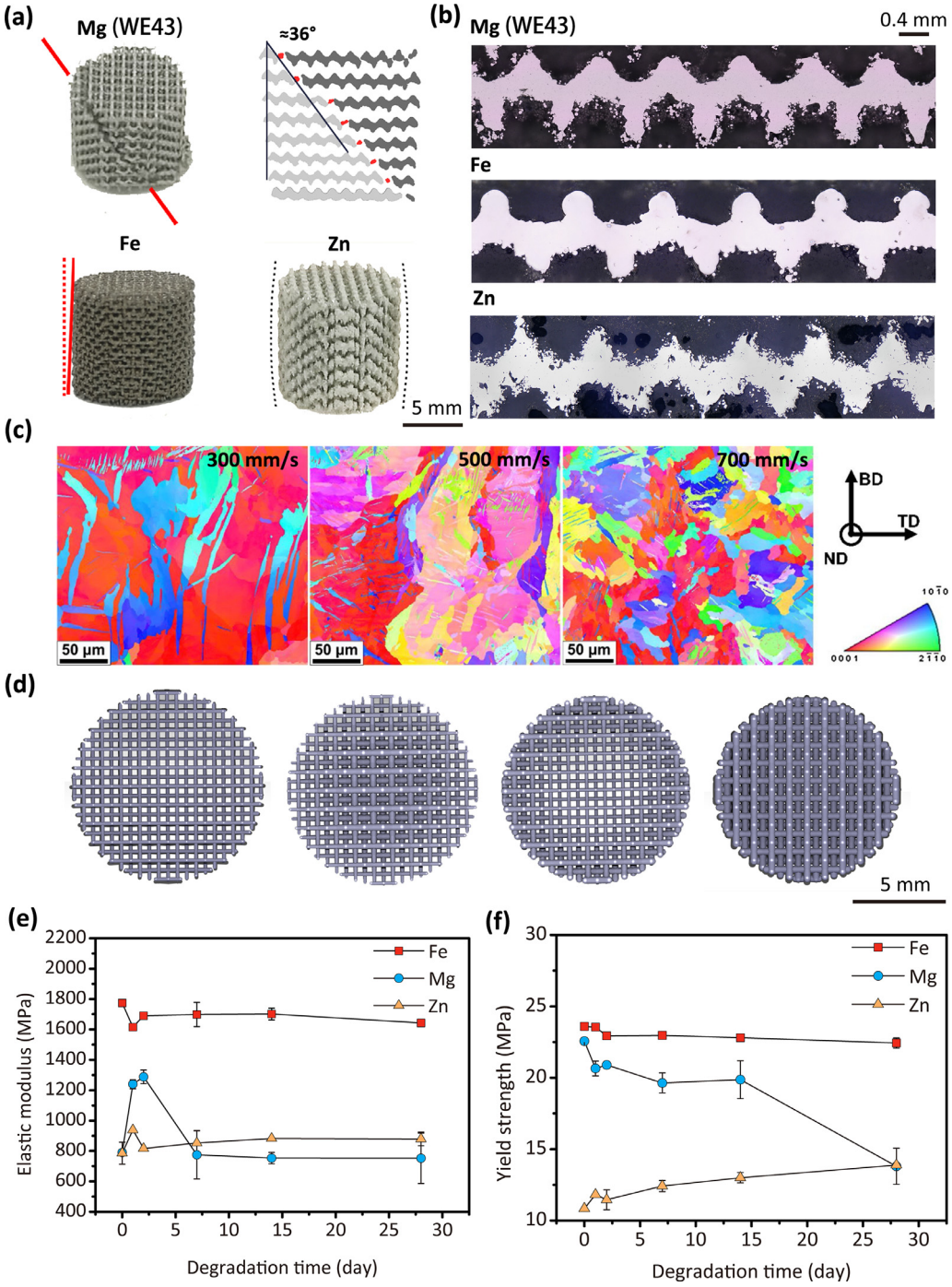

Fig. 2. The mechanical properties of AM biodegradable porous metals: (a) different fatigue failure modes dependent on the material type [86-88], (b) the manufacturing quality of the struts of scaffolds [86-88], (c) the effects of an SLM process parameter on the grain structure of AM zinc [92], (d) the functionally graded designs of AM porous iron [99], and (e,f) the changes in the mechanical properties of the AM magnesium, iron, and zinc scaffolds with *in vitro* biodegradation time [93–95].

has, therefore, been used to polish the surface of AM biodegradable scaffolds [78,93,95,114]. Chemical etching has been found to have only minimal detrimental effects on the compressive mechanical properties of AM biodegradable scaffolds [93,95]. Since sandblasting has been found to improve the fatigue resistance of AM porous titanium [115], it may be used to improve the fatigue resistance of AM biodegradable porous metals as well. Heat treatment can also influence the mechanical properties of AM scaffolds. The compressive strength of SLM WE43 scaffolds was shown to decrease after annealing [116], while SLM iron scaffolds exhibited a higher yield strength after vacuum annealing, as a result of grain refinement [71]. As HIP has been used to improve the ductility and fatigue resistance of AM porous Ti-6Al-4 V [104,117], it is interesting to study the effect of HIP on the mechanical properties of AM biodegradable porous metals. Although coatings on porous biomaterials are normally not aimed for improving mechanical properties, it is necessary to study the effects of coating as well. Plasma electrolytic oxidation (PEO) has been shown to increase the compressive strength of SLM WE43 scaffolds [116]. On the contrary, hydroxyapatite (HA) coating has been found to not significantly affect the mechanical properties of binder-extruded iron scaffolds [118]. It is more relevant to

evaluate the performance of coating under cyclic loading in future studies.

2.5. Biodegradation

The mechanical properties of AM biodegradable porous metals change as the biodegradation process progresses. As expected, SLM porous biodegradable magnesium and iron had decreased yield strengths and stiffnesses after 28 days of *in vitro* degradation in the revised simulated body fluid (r-SBF). However, SLM porous zinc showed even increased mechanical properties as compared to its as-built counterpart after 28 days of *in vitro* biodegradation (Fig. 2e, f) [93–95]. The formation of biodegradation products on SLM zinc scaffolds was found to be responsible for the increase of the mechanical properties, as the biodegradation products were 5 times harder than the base metal (*i.e.*, AM pure Zn) [94].

Biodegradation has a significant influence on the fatigue behavior of AM biodegradable porous metals. Biodegradation has been shown to decrease the fatigue life of SLM porous magnesium and iron [86,88]. Interestingly, the fatigue life of AM porous zinc was even higher after immersion in the r-SBF than in air, which was again attributed to the formation of biodegradation products and their good bonding with AM zinc [87].

As bone implants may be subjected to complex loading conditions in the human body, they need to be tested under a variety of loading regimens including tension and bending. The currently available studies have, however, only focused on the compressive quasi-static mechanical properties and compression-compression fatigue behavior of AM porous biodegradable implants and how biodegradation may affect those.

2.6. General discussion on mechanical properties

Up to now, most AM biodegradable porous metals have shown lower mechanical properties than the human cortical bone (Table 1), making them more suitable for trabecular bone substitution. There are several approaches that can be adopted to improve the mechanical properties of AM porous biodegradable metals. First, for bulk metals, the commonly used strengthening mechanisms include work hardening, solid solution strengthening, precipitation strengthening, grain boundary strengthening, and transformation hardening. Work hardening is mainly attributed to the increased dislocation density mostly through cold working. However, as AM is a net-shape manufacturing technique, only surface hardening, *e.g.*, by means of sand blasting, may be applied to improve the mechanical properties of AM porous metals. In solid solution strengthening, solute atoms can cause lattice distortions that hinder dislocation motion. Alloying can be used to introduce solute atoms to improve the mechanical properties of AM biodegradable metals. Once the concentration of an alloying element is beyond its solid solubility, second-phase particles will form, which can work as pining points for dislocations as well. According to the Hall-Petch relationship, the yield strength is inversely related to the grain size. In the case of SLM, rapid solidification involved in the process leads to the formation of fine grains. The grain size can be adjusted by controlling the thermal history of each layer. Transformation hardening is mainly used for steel, as the level of strength can be controlled by the amount, morphology and structural characteristics of the martensite phase. Hence, it might be useful for AM iron-based alloys, rather than for magnesium- and zinc-based alloys.

Secondly, as the state-of-art AM biodegradable metals still have some internal defects, densification approaches, such as AM process optimization and post-AM heat treatment, are important to improve the mechanical properties of AM biodegradable porous metals. However, it is a significant challenge to identify the optimal process parameters as the final material properties of parts made via SLM are very sensitive to the powder characteristics and physical properties (*e.g.*, powder particle shape, flow characteristics, apparent porosity, laser absorptivity, *etc.*), the geometry of the object, the material composition, and the power source parameters (*e.g.*, beam size, power, scan rate, *etc.*) [119]. Moreover, reliable printing quality requires real-time monitoring of the melt pool and powder bed *in situ*. Machine learning offers a route to predict the process–property relationships and effectively identify the defects [120,121].

Thirdly, lattice structures designed using stretch-dominated unit cells or minimal surfaces should be applied in scaffold design. Currently, most of the PBF biodegradable scaffolds are designed using bending-dominated unit cells (*e.g.*, the diamond unit cell). Functionally graded structures that combine different unit cell types and unit cell sizes need to be developed and studied as well. Considering the fact that there are many different types of unit cells and that the bone structure that needs to be replicated is quite complex [19], it is important to build a database for the mechanical properties of the different porous structures and apply machine learning techniques to relate all the relevant aspects of the design and fabrication processes, including the geometry, process parameters, and the mechanical properties of the resulting objects.

From the mechanical performance viewpoint, AM porous implants should be designed not only with the aim of achieving initially bone-mimicking mechanical properties but also with a proper consideration of how those properties change with time as the biodegradation and bone regeneration processes progress. Printability and the fatigue behavior of such complex structures are the other important considerations. The mechanical design of AM porous biodegradable metals, therefore, requires a much more sophisticated approach than simple mechanical testing according to the standard procedures that are often used in the development of biomaterials.

3. Biodegradation behavior

Given the natural duration of the healing mechanism of the human bone, AM biodegradable implants should provide sufficient mechanical support for 12–24 weeks and be fully absorbed within 1–2 years, depending on the implantation site [69,122]. While it is accepted that bone fixtures are required to have a biodegradation rate < 0.5 mm/year [10], there is no single value that could be used as a criterion for the design of scaffolds. The ideal biodegradation rate of bone substitutes should match the location-dependent rate of bone regeneration [69], which calls for the ability to control the biodegradation rate of porous metals. For AM biodegradable porous metals, the biodegradation behavior can be controlled not only by material type, chemical composition, and microstructure, but also by the geometrical design of the scaffolds. As magnesium generally degrades too fast and iron too slowly, most of the recent research efforts have been directed towards decreasing the biodegradation rate of magnesium and increasing the biodegradation rate of iron. Furthermore, the influence of the loading conditions on the biodegradation behavior of the scaffolds should be considered as well. In the following subsections, we will review and discuss the biodegradation behavior of AM biodegradable bulk and porous metals (Table 2).

3.1. Material type and alloying

The electrode potential values of pure magnesium, iron, and zinc are respectively −2.37 V, −0.44 V, and −0.76 [69], which means that the highest and lowest biodegradation rates respectively belong to magnesium and iron, with zinc occupying an

Table 2
The biodegradation behavior of AM biodegradable porous metals.

Material	Composition	Fabrication method	Unit cell	Porosity	Pore size	Testing medium	Control	Duration	Weight loss	CRI	CRE	Ref.
				%	um				%	mm/year	uA/cm^2	
Criteria	bone fixture									< 0.5 bone fixture		[10]
	stent									< 0.02 stent		[176]
	bone substitute									unknown		
Mg	Mg	SLM				SBF		10	13			[76]
	Mg-1Sn								8			
	Mg-3Sn								15			
	Mg-5Sn								19			
	Mg-7Sn								23			
	AZ61	SLM						6		1–3		[177]
	ZK60	SLM				SBF		7		2	44	[139]
	ZK60–0.2Cu									2	60	
	ZK60–0.4Cu									3	85	
	ZK60–0.6Cu									17	486	
	ZK60–0.8Cu									30	828	
	ZK30	SLM				SBF					131 ± 14	[123]
	ZK30–1Al										68 ± 6	
	ZK30–3Al										24 ± 6	
	ZK30–5Al										156 ± 26	
	ZK30–7Al										340 ± 28	
	Mg-6Zn-0.5Zr					SBF		28		1.6 ± 0.2	36 ± 2	[79]
Fe	Fe	SLM				HANKS					6.2 ± 0.1	[178]
	Fe-2Pd-2.5bredigite	SLM				SBF		21		0.2	18	[138]
	Fe-2Pd-5bredigite							21		0.4	32	
	Fe-2Pd-10bredigite							21		0.5	40	
	Fe-4Pd-2.5bredigite							21		0.4	35	
	Fe-4Pd-5bredigite							21		0.6	50	
	Fe-4Pd-10bredigite							21		0.8	63	
Zn	Zn	SLM				HANKS		21		0.04	2–4	[92]
	Zn	SLM				SBF		21		0.08	8	[80]
	Zn-2Ag					SBF		21		0.09	5	
	Zn-4Ag					SBF		21		0.11	1	
	Zn-6Ag					SBF		21		0.11	10	
	Zn-8Ag					SBF		21		0.13	14	
	Zn-2Al	SLM				SBF		14		0.13–0.16	7–12	[136]
	Zn	SLM				SBF		28		0.18 ± 0.03	9 ± 1	[79]
	Zn-1Mg					SBF		28		0.14 ± 0.01	6 ± 1	
	Zn-2Mg					SBF		28		0.13 ± 0.03	5 ± 1	
	Zn-3Mg					SBF		28		0.10 ± 0.02	4 ± 1	
	Zn-4Mg					SBF		28		0.11 ± 0.04	4 ± 1	

(*continued on next page*)

Table 2 (*continued*)

Material	Composition	Fabrication method	Unit cell	Porosity	Pore size	Testing medium	Control	Duration	Weight loss	CRI	CRE	Ref.
porous Mg	WE43	SLM		76	1131	DMEM	CO_2	21	40			[116]
	WE43+PEO			70	919	DMEM		21	5			
	WE43+PEO			76	1131			21	15			
	WE43+PEO+HT			76	1131			21	39			
	WE43	SLM				HANKS	bioreactor	3	25			[173]
	WE43	SLM	diamond	67	600	r-SBF		28	21	0.2	21–61	[95]
porous Fe	Fe	SLM	cubic	67		SBF		28	5	0.09 ± 0.02	7 ± 3	[85]
	Fe-25Mn								13	0.23 ± 0.05	51 ± 8	
	Fe	3D printing mold+ pressureless microwave sintering	truncated octahedron	81	1580 ± 40	SBF		28	5		61 ± 2	[98]
				60	1450 ± 40				4		88 ± 2	
				46	1170 ± 30				6		141 ± 2	
			cubic	51	1190 ± 20				6		94 ± 3	
	Fe35Mn	SLM	sheet	42	400	HANKS	CO_2&dynamic	28		0.42 ± 0.03	69 ± 2	[84]
	Fe	SLM	diamond	85	800	r-SBF	bioreactor	28	17	0.2		[99]
				70					10	0.14		
				70					9	0.17		
				59	400				5	0.11		
	Fe	SLM	diamond	73		r-SBF		28	3	0.03	103 ± 19	[93]
	Fe	binder extrusion	mesh	66	1000	αMEM		28				[118]
	Fe+HA											
	Fe30Mn	inkjet 3-DP		36		HBSS					58 ± 17	[96]
	Fe-Mn	Binder-jetting 3DP		39		HBSS		28		0.03	2.2 ± 0.4	[97]
	Fe-Mn-1Ca			53						0.14	2.9 ± 0.5	
porous Zn	Zn	SLM	diamond	73	700	r-SBF	bioreactor	28	12	0.17		[100]
				69	graded				8	0.14		
				62	600				7	0.13		
				73	700		static		5	0.07		
				69	graded				3	0.06		
				62	600				4	0.07		
	Zn	SLM	diamond	62	600	r-SBF					45 ± 2	[94]
	Zn	3D printed templates + casting		20	900	Hank's				0.13		[175]
				60	2000					0.15		

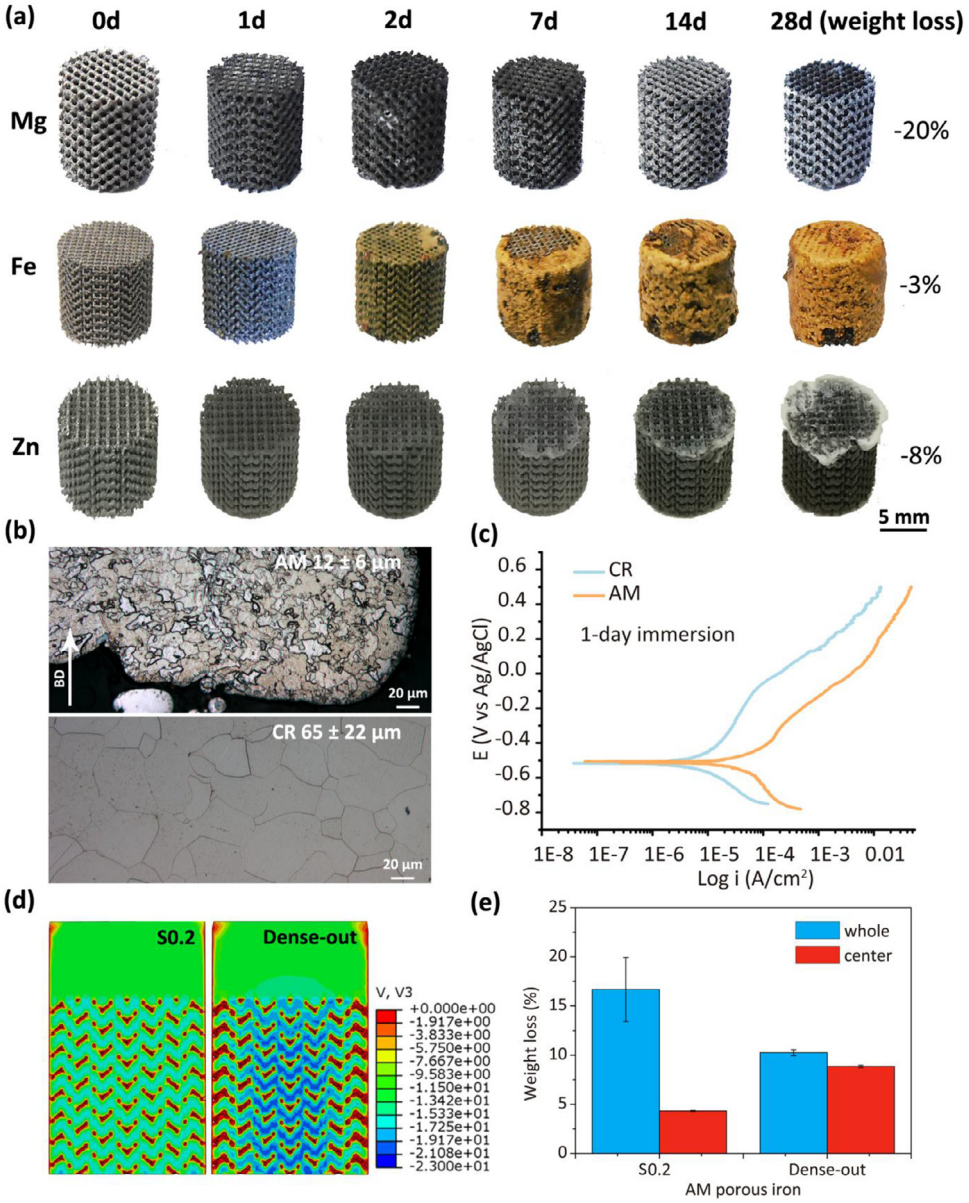

Fig. 3. The biodegradation behavior of AM biodegradable porous metals (Mg, Fe, and Zn): (a) the morphologies of samples after *in vitro* immersion tests at different time points [93–95], (b-c) the microstructures of AM iron and cold-rolled iron (b), and a comparison between the biodegradation behavior of the different materials based on the results of electrochemical tests (c) [93], (d) the flow distributions in uniform and functionally graded structures according to CFD modeling, and (e) the effects of geometrical design on the biodegradation behavior of AM porous iron [99].

intermediate position. Li et al. [95] showed that, after 28 days of *in vitro* biodegradation, AM WE43 scaffolds had lost ≈ 20% of their weight. Within the same time period, AM zinc and iron exhibited 8% and 3% of weight loss, respectively (Fig. 3a).

Alloying is frequently used to tune the biodegradation behavior of AM scaffolds. On the one hand, alloying can lead to grain refinement, which can improve the biodegradation resistance of magnesium. On the other hand, alloying can generate second phase(s) or cause grain boundary segregation, which can accelerate galvanic degradation. In one study, for example, the biodegradation rate of SLM magnesium decreased when it was alloyed with 1% Sn, while a higher percentage of added tin increased the biodegradation rate of the material [76]. This is due to the fact for Sn contents exceeding >1%, the influence of second phase(s) overshadows that of grain refinement. Similar results have been obtained for SLM ZK30 alloy added with aluminum [123]. For iron, Shuai et al. [85] and Carluccio et al. [84] have shown that an AM FeMn alloy had a higher biodegradation rate than AM pure iron, because of increased galvanic degradation. For zinc, the addition of silver increased the biodegradation rate, while added magnesium increased the biodegradation resistance [79,80], which was attributed to the different impacts of grain refinement and second phases in each case.

3.2. AM processing

As discussed above in SubSection 2.3, AM processes lead to the formation of some unique defects and microstructures, which can affect the biodegradation profile of the resulting material. Li et al. [93] found that SLM iron with fine grains had a much higher biodegradation rate than cold-rolled iron with a larger grain size (Fig. 2b, c), which is contrary to AM magnesium. Ralston et al. [124] suggested that the relationship between the grain size and the rate of biodegradation is dependent on the level of passivity

on the metal surface. Different AM process parameters lead to different grain structures, which can also affect the biodegradation rate, as shown in the case of SLM zinc fabricated using different scanning speeds [92]. To date, only two studies have been conducted regarding the effects of the grain size on the biodegradation rate of zinc. The corrosion rate of zinc has been found to increase when the grains are refined, which is a result of higher grain boundary densities [92,125], while nanocrystalline zinc has shown good biodegradation resistance [126]. AM-related residual stress can also affect the biodegradation rate of AM porous metals. Considering different AM approaches, as binder extrusion creates a porous structure within the struts, it is expected that the scaffolds made with binder extrusion will show a higher biodegradation rate than those made with PBF techniques.

3.3. Geometrical design

Unlike bulk biodegradable metals, AM biodegradable porous metals show a strong location-dependent biodegradation behavior. After 28 days of *in vitro* degradation, AM porous magnesium showed more localized biodegradation in the center than on the periphery of the scaffolds [95]. The accumulation of biodegradation products between the struts created relatively narrow spaces that could lead to limited diffusion of Mg ions in the center, leading to crevice-like corrosion. AM porous zinc has been found to exhibit localized biodegradation at the bottom of the specimens, where they were in contact with the beaker [94]. The localized biodegradation was attributed to the flow stagnation caused by the narrowness of the space available for fluid flow. For AM porous iron, however, *in vitro* degradation occurred more on the periphery of the scaffolds than in the center [93]. Li et al. [99] used geometrical design to control the biodegradation rate of AM porous iron (Fig. 2d, e). It was found that the biodegradation rate of AM porous iron is correlated with the scaffold porosity and that functionally graded designs could be used to tune the biodegradation profile of the scaffolds. Similar observations have been made for AM functionally graded porous zinc [100].

3.4. Post-AM treatments

Surface roughness is believed to affect the biodegradation rate of biodegradable metals [127]. As PBF specimens normally have adhered powder particles on their struts, smoothening the surface can change the corrosion profile of such biomaterials, especially at the beginning when the specimens come in contact with a (simulated) physiological solution for the first time. The polishing procedures applied so far, including chemical etching, electrochemical etching, and sandblasting, have not been successful in achieving homogeneous, smooth surfaces on the periphery and in the center of the scaffolds [93,95]. Inhomogeneous surface finish within a scaffold may lead to different location-dependent biodegradation profiles. Moreover, as discussed in SubSection 2.4, sandblasting can induce stress concentration, which can affect the biodegradation rate as well.

Other more advanced (electro)chemical treatments could also be used to adjust the biodegradation profile of AM porous metals. For example, Kopp et al. [116] found that application of PEO treatment to AM WE43 scaffolds could significantly decrease their biodegradation rate, while heat-treated specimens showed impaired biodegradation performance. HA coating on AM iron scaffolds are found to decrease the release of Fe ions during *in vitro* biodegradation tests [118].

3.5. Mechanical loading

Dynamic loading significantly increases the biodegradation rates of AM biodegradable porous magnesium, iron, and zinc [86–88]. The biodegradation products formed on the surface of the scaffold struts could fall off under cyclic loading, particularly given that their mechanical properties are very different from those of the metallic substrate. In addition, dynamic loading could increase the possibility of pitting occurring to AM biodegradable porous metals [86,88]. The extrusion and intrusion of persistent slip bands occurring during cyclic loading could break up the corrosion product layer present on the surface of the specimens [128]. In addition, pitting potentials have been found to be much smaller under cyclic loading than those without an imposed stress [129–132]. Finally, the pitting potentials decrease with an increasing stress level [129–132]. As a result of those mechanisms, the biodegradation rate has been found to increase with the loading force [86–88].

3.6. General discussion on biodegradation behavior

It is currently unclear whether the biodegradation rates of AM biodegradable porous metals measured using *in vitro* test protocols are too high or too low, as there is no *in vivo* data available and the correlations between the *in vitro* and *in vivo* data are unknown. For bulk magnesium, *in vitro* degradation rates are normally 1–4 times higher than the values obtained *in vivo*, depending on the alloy and the *in vitro* testing conditions [133]. Despite the absence of *in vivo* data for AM biodegradable porous metals, it is still meaningful to understand how the *in vitro* biodegradation behavior is affected by the chemical composition, microstructure, geometrical design, and surface conditions of the porous structures. Such an understanding would enable the development of effective approaches for adjusting the biodegradation rates of AM porous metals, when needed. Given the fact that there are so many variables that may affect the biodegradation behavior of AM biodegradable porous metals, it may be more efficient to create a biodegradation database and apply machine learning techniques to predict the biodegradation rates of various types of designs in the future [134]. In general, when evaluating the biodegradation behavior of AM biodegradable porous metals, it is useful to report the biodegradation rates in terms of weight loss percentages in addition to expressing them in terms of mm/year. The unit mm/year is normally applied to bulk biodegradable metals. For porous structures, the ratio of the surface area to weight is much higher than their bulk counterparts. Moreover, this ratio changes all the time as the biodegradation process progresses.

4. Biocompatibility

The *in vitro* biocompatibility of bulk biodegradable metals has been extensively studied. AM biodegradable porous metals have microstructures and geometrical features that are different from their bulk counterparts. This can affect their cell responses both directly and indirectly by influencing the biodegradation behavior. Up to now, only a few studies have been conducted on the *in vitro* biocompatibility of AM biodegradable porous metals (Table 3).

4.1. Material type and alloying

Li et al. [93–95] determined the cytocompatibility of AM biodegradable porous metals *in vitro* using MG63 cells and 10X diluted extracts. AM porous WE43 magnesium alloy and zinc respectively showed $< 25\%$ and $< 15\%$ non-viable cells (*i.e.*, level 0 cytotoxicity) after 72 h of *in vitro* biodegradation. In comparison, the cytotoxicity of AM porous iron reached 40% (*i.e.*, level 1 cytotoxicity) after 72 h (Fig. 4a). Witte et al. [135] showed that AM porous

Table 3
The biocompatibility of AM biodegradable porous metals.

Material	Composition	Fabrication method	Unit cell	Porosity %	Cell line	Biocompatibility				Staining/SEM		Ref.
						Area to volume ratio	concentration	Duration (Day)	Viability (%)	method	results	
Mg	ZK60	SLM			MG63	1.25 cm^2 mL^{-1}	100%	1	102			[139]
	ZK60–0.2Cu								103			
	ZK60–0.4Cu								101			
	ZK60–0.6Cu								100			
	ZK60–0.8Cu								98			
	ZK60	SLM						5	95			
	ZK60–0.2Cu								92			
	ZK60–0.4Cu								90			
	ZK60–0.6Cu								82			
	ZK60–0.8Cu								79			
Fe	Fe-2Pd-2.5bredigite	SLM			MG63	1.25 cm^2 mL^{-1}	100%	3	127	well plate	High cell densities after 5 days. The number of live cells slightly decreased as the Pd content increased.	[138]
	Fe-2Pd-5bredigite								106			
	Fe-2Pd-10bredigite								93			
	Fe-4Pd-2.5bredigite								81			
	Fe-4Pd-5bredigite								93			
	Fe-4Pd-10bredigite								94			
Fe	Fe-2Pd-2.5bredigite	SLM						5	127			
	Fe-2Pd-5bredigite								107			
	Fe-2Pd-10bredigite								90			
	Fe-4Pd-2.5bredigite								85			
	Fe-4Pd-5bredigite								91			
	Fe-4Pd-10bredigite								108			
Zn	Zn-2Al	SLM			MG63	1.25 cm^2 mL^{-1}	100%	1	67	well plate		[136]
								4	78			
								7	86			
							50%	1	81			
								4	89			
								7	92			
	Zn	SLM			MG63	1.25 cm^2 mL^{-1}	100%	1	66	well plate	Favorable cell spreading and proliferation until day 3, more cells on Zn-Mg alloy.	[79]
	Zn-1Mg								68			
	Zn-2Mg								67			
	Zn-3Mg								74			
	Zn-4Mg								75			
	Zn	SLM					100%	5	76			
	Zn-1Mg								83			
	Zn-2Mg								86			
	Zn-3Mg								91			
	Zn-4Mg								92			
	Zn	SLM					50%	1	85			
	Zn-1Mg								91			
	Zn-2Mg								92			
	Zn-3Mg								93			
	Zn-4Mg								94			
	Zn	SLM					50%	5	91			
	Zn-1Mg								98			
	Zn-2Mg								110			
	Zn-3Mg								123			
	Zn-4Mg								121			

(*continued on next page*)

Table 3 (*continued*)

Material	Composition	Fabrication method	Unit cell	Porosity	Cell line	Biocompatibility				Staining/SEM		Ref.
				%		Area to volume ratio	concentration	Duration (Day)	Viability (%)	method	results	
porous Mg	WE43	SLM			hOB		100%	3	100			[173]
	WE43	SLM	diamond	67	MG63		10%	1	75	specimen	Few viable (green) cells were detectable on WE43 after 1 day.	[95]
								2	97			
								3	88			
	Fe	SLM	cubic	67	MG63	1.25 cm^2 mL^{-1}	100%	1	79		Few dead cells were observed and adhered cells on scaffold clearly increased from day 1 to day 3.	[85]
								3	84			
								5	92			
	Fe-25Mn						100%	1	69			
								3	71			
								5	75			
	Fe-25Mn						50%	1	79			
								3	85			
								5	92			
	Fe	3D printing mold+ Pressure-less Microwave Sintering	truncated octahedron	81	mouse fibroblast 3T3	2.5 cm^2 mL^{-1}	100%	1	89	specimen	After 24 h, only a limited number of cells were found. There is an effect of geometry variation on cell viability.	[98]
				60					88			
				46					84			
			cubic	51					86			
			truncated octahedron	81	fibroblast 3T3		100%	3	60			
				60					55			
				46					44			
			cubic	51					49			
			truncated octahedron	81	fibroblast 3T3		50%	3	95			
				60					92			
				46					83			
			cubic	51					86			
	Fe35Mn	SLM	sheet	42	MC3T3-E1 (Pre-osteoblast	1.25 cm^2 mL^{-1}		1	114	specimen	After 4 h, filopodia were formed and attached on the scaffolds	[84]
								3	103			
	Fe	SLM	diamond	85		0.2 g/ml	10%	1	78	specimen	24 h after seeding, well-spread polygonal cell morphology with cytoplasmic projections were observed.	[99]
				70					79			
				70					82			
				59					87			
				85				3	43			
				70					47			
				70					50			
				59					46			
	Fe	SLM	diamond	73		0.2 g/ml		1	75	specimen	After 24 h, viable cells were hardly detectable on iron	[93]
								3	40			
	Fe	binder extrusion	mesh	66	rBMSCs		100%			specimen	All cells dead after 1 day	[118]
	Fe+HA										A higher density of live cell attachment after 3 days	
	Fe30Mn	inkjet 3DP		36	MC3T3-E1	0.2 g/ml	100%	1	46	specimen	Higher cell density in day 3 than day 1.	[96]
								3	81			
							10%	1	82			
								3	99			
	Fe-Mn	Binder-jetting 3DP		40	MC3T3	0.2 g/ml	100%	3	81	specimen	Higher cell density in day 3 than day 1. Substantial cell-cell junctions and cytoplasmic extension.	[97]
							50%		115			
							10%		117			
	Fe-Mn-1Ca			53			100%	3	116			
							50%		132			
							10%		112			
porous Zn	Zn	SLM	diamond	73	MG63		10%	1	99	specimen	After 1 d, most of MG-63 cells were viable.	[100]
				69					97			
				62					98			
				73				3	91			
				69					88			
				62					85			
	Zn	SLM	diamond	62	MG63	0.2 g/ml	10%	1	95	specimen	After 1 d, most of cells were viable. Far-stretching filopodia-like protrusions.	[94]
								2	95			
								3	85			
	Zn	SLM	diamond		hTERT-MSCs					specimen	After 13 d, no indication of cell attachment and growth	[103]
	Zn	3D printed templates + casting		20	MC3T3-E1	1.25 cm^2 mL^{-1} (outside dimensions)	100%	1	10	specimen	After 1 d, flat morphology with numerous filopodia extensions	[175]
								5	2			
							10%	1	95			
								5	88			
				60			100%	1	10		Slightly round morphology and cell nuclei with elongated cell bodies	
								5	3			
							10%	1	80			
								5	71			

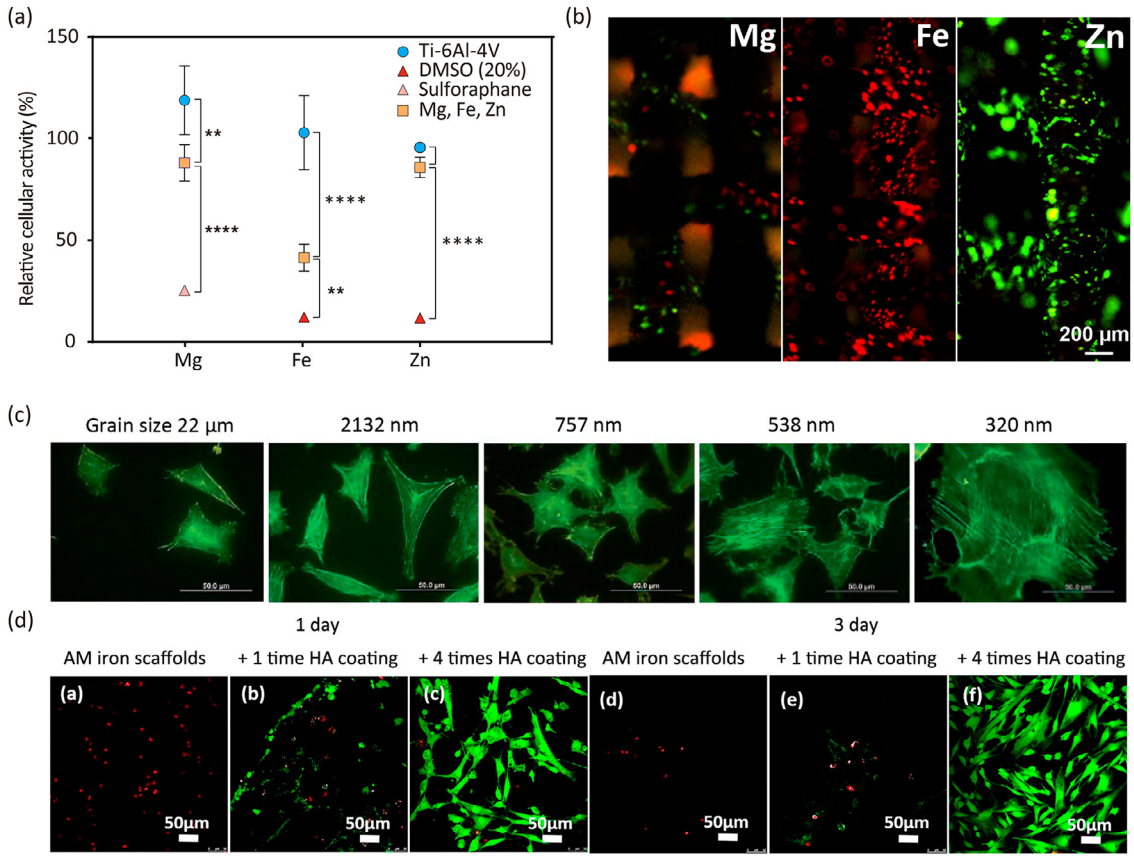

Fig. 4. The *in vitro* biocompatibility of AM biodegradable porous metals: (a) the indirect cytotoxicity tests of AM biodegradable porous metals using MG63 cells after 72 h [93-95], (b) the direct live/dead staining tests performed using the MG63 cells after 24 h [93-95], (c) the fluorescence micrographs of the actin stress fibers of MC3T3 pre-osteoblast cells cultured on austenitic stainless steel with different grain sizes after 48 h of culture [141], and (d) the live/dead staining of rBMSCs cells after 1 and 3 days of culture on AM porous iron [118].

WE43 magnesium alloy exhibited high degrees of cytocompatibility with up to 100% viability of human osteoblasts (hOB) even with undiluted extracts were used. Shuai et al. [79] used MG63 cells to study the cytocompatibility of AM bulk zinc after 5 days of biodegradation and found > 75% and > 90% cell viability with undiluted and 2X diluted extracts, respectively. However, Lietaert et al. [103] have reported a low degree of compatibility (*i.e.*, viability) of human telomerase reverse transcriptase mesenchymal stem cells (hTERT-MSCs) with AM zinc scaffolds. The cytocompatibility of AM porous iron is uncertain too. Shuai et al. [85] found that, in the case of AM porous iron, the viability of MG63 increased with culture time and reached values > 90% after 5 days. On the other hand, Yang et al. [118] found that most of the rabbit bone marrow mesenchymal stem cells (rBMSCs) were dead on AM Fe scaffolds after 3 days. Similar result has been presented by Li et al. [93] who found most of the MG63 cells are dead directly after seeding on AM Fe scaffolds.

Alloying with different elements has had varied effects on the biocompatibility of AM biodegradable porous metals. For example, AM Zn-3Mg has shown improved cell viability as compared with pure Zn [79]. AM Zn-2Al has also shown >85% viability with MG63 cells after 7 days [136]. Manganese is the most commonly used alloying element for AM porous iron. Most of the studies have shown that AM Fe-Mn alloys exhibit good biocompatibility, although Shuai et al. [85] found that Mn slightly decreased cell viability when compared with AM pure iron [84,97,137]. AM Fe-Pd-bredigite composites [138] have shown increased biocompatibility with higher bredigite content, but decreased biocompatibility with higher Pd content. Fe-Mn-Ca also showed >100% viability with MC3T3-E1 cells after 3 days [97]. A small amount of Cu added to AM bulk ZK60 decreased its biocompatibility as measured using the viability of MG63 cells but created an antibacterial effect against Escherichia Coli [139].

The indirect cytotoxicity of a material is related to the ion concentrations of the elements involved. Hong et al. [140] compared the viability of the osteoblastic cell line MC3T3-E1 with Fe, Mn, Ca, and Mg salt in culture medium at 0.1, 1, and 10 mM concentrations after 7 days of culture and found that Fe and Mn had >75% cytotoxicity for a concentration as little as 1 mM. It can, thus, be inferred that one of the reasons for the inconsistent results concerning the cytocompatibility of AM porous metals is the differences in the released ion concentration. It is, therefore, proposed that in future indirect cytocompatibility tests, ion concentrations be determined and reported.

Direct cytotoxicity tests of AM porous metals generally provide a harsher environment for cells, as the local pH and ion concentrations can be much higher than those of the culture medium. Indeed, Li et al. [93] found that most of MG63 cells were dead on AM porous pure iron and few viable cells were detectable on AM porous WE43 alloy after 24 h (Fig. 4b). Similar to the indirect cytotoxicity tests, inconsistent results have been reported by different research groups with the same material type and the same cell lines. Shuai et al. [85] showed that only a few dead MG63 cells were detected on AM porous iron and the cell density even increased from day 1 to day 3. AM porous zinc showed good direct biocompatibility with MG63 cells after 1 day [94], while the low viability of hTERT-MSCs on Zn scaffolds was confirmed by their low rate of lactate production and the DNA measurements [103].

Round-robin tests and different cell types are, thus, needed in the future to more rigorously and conclusively evaluate the *in vitro* biocompatibility of AM porous metals.

4.2. AM processing

AM processing can affect cell activity through different pathways. As the chosen AM process and processing parameters affect the grain sizes and grain structure of a 3D printed material, AM processing logically plays an important role in mediating cell responses [141]. Saha et al. [142] found that both proliferation and differentiation of MC3T3 cells improves when the grain size of magnesium is reduced. Sunil et al. [143] observed that biomineralization, cell adhesion, and proliferation on the AZ91 magnesium alloy was improved through grain refinement, because the improved wettability of the alloy with refined grains could promote protein adsorption, which in turn helped cell attachment and proliferation. Nie et al. [144] showed that nanocrystalline pure iron stimulated the proliferation of fibroblast cells and promoted endothelialization, while effectively inhibiting the viability of vascular smooth muscle cells (VSMCs). Similar results have been obtained for Ti-6Al-4 V and Co-Cr-Mo alloys (Fig. 4c) [145], in which enhanced osteoblast performance has been attributed to enhanced protein adhesion. However, unlike bioinert metals, grain refinement also affects the biodegradation rate of biodegradable metals, making it challenging to deconvolute the biological effects of biodegradation rate and grain size and the eventual cell response. More systematic studies are needed to elucidate the fundamental mechanisms that govern the responses of cells to biodegradable metals with different grain sizes. This would allow for modifying the cytocompatibility of AM biodegradable porous metals through the adjustment of grain sizes.

4.3. Geometrical design

The effect of geometrical design on the cell responses to AM porous titanium has been extensively studied. The porosity and pore size have been found to significantly affect the cell response. Pore size has been shown to influence the flow of nutrients and waste and, thus, cell activity in the center of the scaffolds. Moreover, it has been found that a smaller pore size can cause cell clogging within the porous structure of the scaffold during the initial time period after the start of cell culture, thereby disrupting cell growth [146]. Pore shape could also affect cell proliferation for Ti-6Al-4 V scaffolds, with triangular pores showing enhanced cell proliferation as compared to hexagonal and rectangular pores [147]. For biodegradable metallic scaffolds, AM porous iron and zinc have shown different cell seeding efficiencies with different porosities [99,100]. To date, no study has been performed to investigate the influence of geometrical design on the responses of cells to AM biodegradable scaffolds. As compared with the bioinert metals discussed above, there is another mechanism to consider in the case of biodegradable metals: Geometry can also affect the biodegradation behavior of the scaffolds, thereby influencing their cell responses. Future studies should consider the effects of porosity, pore size, and pore shape on the cell responses of AM biodegradable porous metals both in their own right and in relation with the effects that those parameters have on the biodegradability of such biomaterials. Such an understanding is essential for optimizing the geometrical design of biodegradable porous structures.

4.4. Post-AM treatments

Surface treatment can influence the cytocompatibility and general cell response of AM biodegradable scaffolds. For example, calcium phosphates (CaPs) coatings have similar compositions to the bone mineral component, which is why they afford magnesium-based scaffolds with excellent osteoconductivity and bioactivity [148]. Similarly, HA coating has been found to improve the biocompatibility of AM porous iron (Fig. 4d) [118]. A similar observation has been made for ZnP coating applied to zinc [149]. To date, only a few researchers have investigated the effects of coatings on the biocompatibility of AM biodegradable porous metals. Many organic and polymeric coatings can be developed to further improve the biocompatibility of AM biodegradable porous metals. Being different from bulk biodegradable metals, it is challenging to make the coating homogeneous throughout AM biodegradable porous metals, especially in the center.

4.5. General discussion on biocompatibility

In vitro biocompatibility tests are useful for material screening before *in vivo* tests in the animal model are performed. AM porous metals generally have much higher surface area and, thus, higher biodegradation rates than their bulk counterparts. When choosing the volume of the cell culture medium, considering the surface/volume ratio makes more mechanistic sense than basing the calculation on the weight/volume ratio, especially for direct biocompatibility tests. Although *in vitro* cell responses to AM magnesium, iron, and zinc ions are mainly affected by the released ion concentrations and pH, it is necessary to consider the total released ions per day. The recommended daily allowances of magnesium, iron, and zinc for human are 420, 8, and 11 mg, respectively [150].

5. Bone formation

Given that AM biodegradable porous metals have appeared in the literature very recently, only a few *in vivo* studies have been carried out so far. Here, we summarize and discuss the results reported to date in relation with the material type, geometry, and post-AM treatments.

5.1. Material type

Witte et al. [43] found that AZ91 magnesium scaffolds could promote both peri–implant bone formation and bone resorption in a rabbit model, leading to a higher bone mass and more mature bone around the degrading magnesium scaffolds than autologous bone. In a different study, 3D printed PLGA/TCP/Mg scaffolds showed 56.3% higher mean bone volume than the PLGA/TCP group (Fig. 5a) [151]. With the incorporation of Mg, PLGA/TCP/Mg scaffold not only offered suitable template for vessel creeping but also promoted neoangiogenesis. Furthermore, open porous LAE442 (Mg-4%Li-3.6%Al-2.4%RE) scaffolds have shown comparatively better osseointegration with more trabecular contacts than La2 scaffolds [152].

SLM iron-manganese scaffolds have been found to exhibit osteointegration after 4 weeks in rat cranial bone, where bone apposition was found on the scaffold (Fig. 5b) [84]. Micro-CT showed new bone formation in the scaffolds. Although there is currently no information available regarding the *in vivo* performance of porous zinc, bulk zinc has shown good biocompatibility *in vivo* [153–155]. Xiao et al. [156] found new bone formation after implanting Zn in the femoral shaft of a rabbit for 12 weeks. Li et al. [157] showed that Zn-1X (X = Mg, Ca, Sr wt%) pin in the femora of mice had significantly larger new bone thickness than the sham control group after 8 weeks.

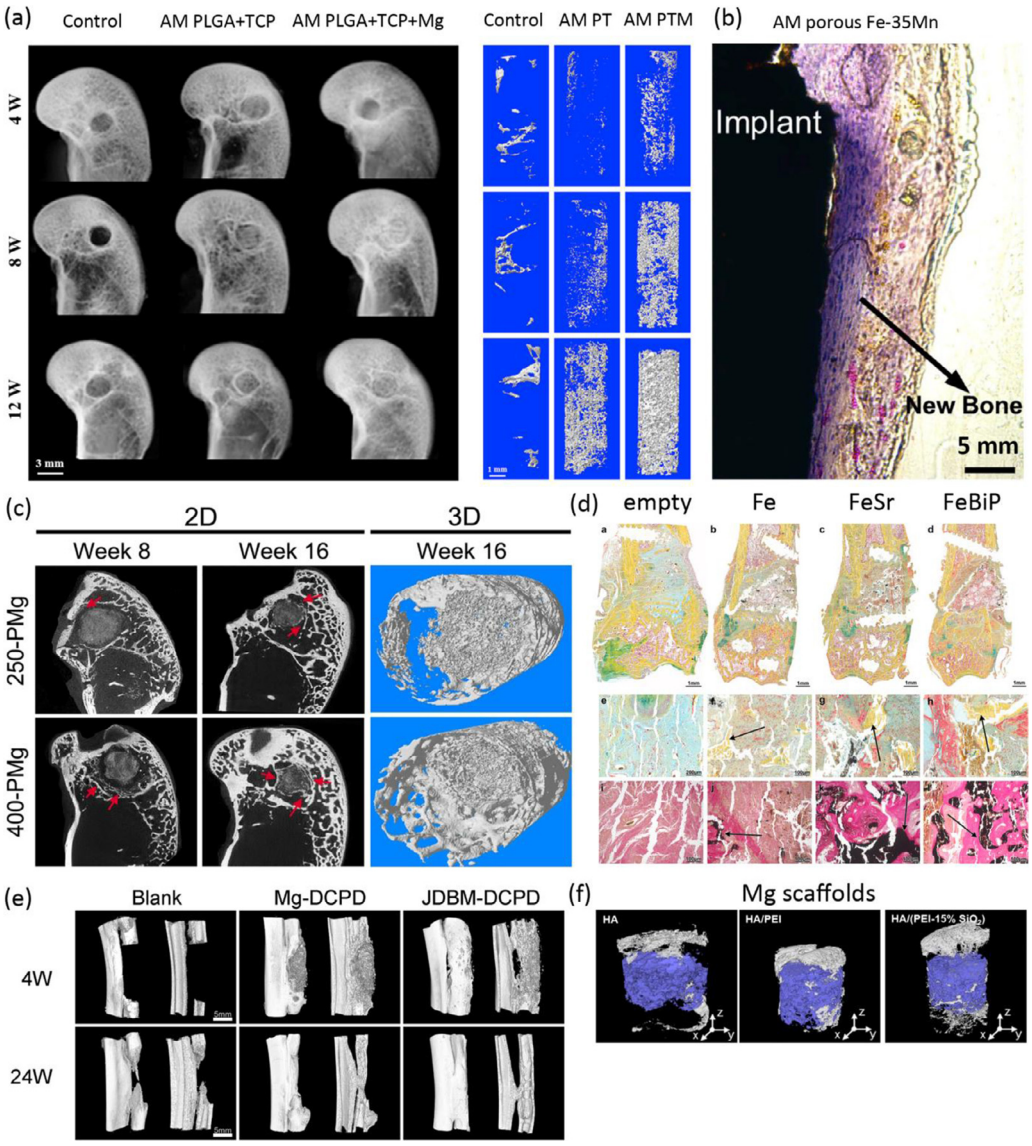

Fig. 5. The *in vivo* performance of AM biodegradable porous metals: (a) the representative radiograph and 3D micro-CT images of new bone formation within bone tunnel at 4, 8, and 12 weeks after the implantation of AM PLGA/TCP/Mg scaffold [151], (b) a histological image of AM porous Fe-35Mn in bone and new bone formation on the surface of the scaffolds [84], (c) micro-CT 2D (the red arrows refer to the newly formed bone) and 3D reconstruction models showing the status of *de novo* bone formation (white in color) 16 weeks after the implantation of Mg scaffolds, (d) a histomorphometrical analysis of new bone formation in the initially created defect zones when they were left empty or were treated through the implantation of Fe, FeSr, or FeBiP scaffolds [161], (e) the micro-CT images of *de novo* bone after 4 and 24 weeks of surgery for blank, Mg-DCPD, and JDBM-DCPD scaffolds [41], (f) a 3D reconstructed model of the bone tissue and the implant 10 weeks after the surgery (white: bone, violet: specimen) and following the implantation of HA-, HA/PEI-, and HA/(PEI-15% SiO_2)-coated porous Mg [50].

5.2. Geometrical design

Pore size has been shown to influence bone ingrowth into bioinert scaffolds, although the effect is still controversial in the literature [19]. Braem et al. [158] observed new bone formation in a microporous titanium coating implanted in the compact bone of rabbit tibiae with a pore size $<$ 10 μm. Bai et al. [159] suggested that the upper limit of pore size for vascularization was 400 μm beyond which increased pore size showed no significant difference. However, Naoya et al. [160] have found that, in rabbit tibia, titanium scaffolds with a pore size of 900 μm demonstrate significantly higher bone ingrowth than 300 μm scaffolds. Only a few studies have reported the effects of the geometry of biodegradable porous metals on bone formation. With the same porosity, magnesium scaffolds with a larger pore size were found to promote vascularization and led to higher bone mass and more mature bone formation in a rabbit model (Fig. 5c) [27]. It is, therefore, important to consider the influence of geometrical design on the biodegradation rate and the formation of biodegradation products of AM biodegradable porous metals.

5.3. Post-AM treatments

Post-AM treatments could affect the bone regeneration performance of biodegradable metals. For example, dual coating on magnesium scaffolds, particularly the SiO_2 hybrid dual coating has been reported to stimulate bone regeneration at the defect site (Fig. 5f) [50]. In another study, fluoride-pretreated AZ31 scaffolds were more biocompatible and induced significantly more new bone formation *in vivo* than the same scaffolds without a MgF_2 coating [46]. Moreover, the Brushit (DCPD) coating has been shown to significantly increase the vascular regeneration ability of Mg–Nd–Zn–Zr (JDBM) scaffolds, which was also accompanied by more bone growth and bone integration (Fig. 5e) [41]. In yet an-

other study, Ray et al. [161] have reported that iron scaffolds with a FeSr coating result in significantly increased bone formation as compared to a FeBiP coating and bare iron after 6 weeks of implantation in rat femur (Fig. 5d). Finally, Yang et al. [162] have reported that the addition of HA to zinc results in improved osteogenic performance with prolonged implantation time in the rat femoral condyle. There is, therefore, ample evidence suggesting that AM biodegradable porous metals with appropriate coatings will offer enhanced bone regeneration performance as compared to their bare counterparts.

5.4. General discussion on bone formation

Although there have been only a few studies on the *in vivo* bone regeneration performance of biodegradable porous metals, *de novo* bone formation has been found in all the studies. Compared to Mg and Zn, which are natural nutrients in the bone, the use of Fe as a biodegradable bone implant material is debatable in the literature, considering its cytotoxicity and non-biodegradable byproducts on the one hand [163] and its deficiency, leading to a variety of disorders on the other [164]. Despite this debate, many research groups have been studying iron-based biomaterials and exploring its use for orthopedic treatments [84,161,165]. AM biodegradable porous metals can interact with the human body through both biophysical and biochemical properties. Biophysical properties include stiffness, porosity, topography, and degradation rate, which can influence the local tissue microenvironments and, thus, control the presence of enzymes, cells, ions, or radical species [166]. For example, the stiffness of the scaffolds can dictate the adhesion, spreading, and fate of bone marrow cells, in which stiffer surface directs stem cells into osteogenic lineages, while softer surface promotes chondrogenic differentiation [167]. The appropriate porosity of the scaffold can facilitate the transport of nutrients, oxygen, and waste products and promote vascularization. Similarly, surface features (patterns) may promote or suppress cell adhesion and cell fate [21]. Additionally, the rate of biodegradation should match the rate of bone tissue regeneration for optimal tissue growth. The relevant biochemical properties include the dissolution of the AM scaffolds itself and the released functional molecules or ions from coating and substrate, which can also alter the tissue microenvironment and thus modulate the regeneration process. For example, magnesium has been found to promote calcitonin gene-related polypeptide-α (CGRP)-mediated osteogenic differentiation [168]. More *in vivo* studies are needed to evaluate the bone tissue regeneration performance of AM biodegradable porous metals, considering the effects of chemical composition, geometrical design, and coating. Moreover, longer *in vivo* tests are needed to not only evaluate the bone regeneration performance and the rate of biodegradation of AM biodegradable porous metals but also to obtain information regarding the fate of the biodegradation products.

6. Conclusions and future research directions

With proper geometrical design, alloying, processing, and surface treatment, AM biodegradable porous metals could emerge as a new generation of functional biomaterials that are particularly useful as bone substitutes and could greatly facilitate the treatment of large bony defects. This will further expand the range of biomaterials that are available for orthopedic treatments, although there are still many applications, where non-biodegradable materials need to be used. There are, however, many areas of research that need to be addressed before such a goal is achieved. Some of those areas are highlighted in what follows as potentially interesting future research directions.

i Mechanical properties: The quasistatic mechanical properties of AM biodegradable porous pure metals are within the range of the values reported for the human trabecular bone, while being lower than those of the human cortical bone. AM porous iron exhibits better mechanical properties than AM porous magnesium and zinc. AM process optimization, alloying, and geometrical optimization can be used to further improve the quasistatic mechanical properties of AM biodegradable metallic scaffolds. The studies addressing the corrosion fatigue behavior of AM biodegradable porous metals are still limited in number and scope. AM porous pure zinc and iron showed much better corrosion fatigue resistance than AM porous magnesium. The fatigue behavior of AM porous metal can be further improved by optimizing both the geometrical design of the porous structure and the PBF process parameters, which determine the microstructure of the resulting AM material. As far as mechanical testing is concerned, the creep and aging of AM zinc-based biomaterials and their relationship with the time-dependent performance of orthopedic implants need to be further investigated. Moreover, different loading regimens, such as compression-tension, tension-tension, bending, and torsion, should be applied to AM biodegradable porous metals, depending on the loading condition during the intended use.

ii Biodegradation behavior: The optimum *in vitro* biodegradation rate for AM biodegradable porous metals is not settled yet, as there is currently only limited data available from *in vivo* studies to allow the correlations to be established. For the same porosity, AM biodegradable porous magnesium showed a higher *in vitro* biodegradation rate than AM biodegradable porous iron, with AM biodegradable porous zinc in between. The biodegradation rate can be controlled by AM processing, composition, geometrical design, and coating, which affect the rate of biodegradation in a complicated and inter-related manner. Machine learning including deep learning algorithms may be used to create predictive models that quantify the complex relationships between the chemical composition, process parameters, the microstructure of the processed materials, the geometry of the lattice structures, the resulting mechanical properties, and the biodegradation profile of AM porous biodegradable metals. Such an approach could eventually lead to the establishment of the materials “genome”, which can guide the development of future AM porous biomaterials and replace the currently used trial-and-error approach. More specifically, this methodology should be used to study the effects of microstructure, including grain size, on the biodegradation behavior of AM biodegradable metals.

As far as specific material types are concerned, it would be interesting to explore the potential of AM Mg-based porous metallic glasses and their relevant process parameters. This approach could result in AM Mg-based porous biomaterials with simultaneously improved biodegradation resistance and mechanical properties. As for iron-based materials, the alloying of pure iron with other elements should be considered for both improving the mechanical properties and further increasing the biodegradation rate of AM Fe-based porous biomaterials. Regarding Zn-based AM porous biomaterials, alloying Zn with other elements, particularly Mg and Li, should be applied to improve the mechanical properties of the resulting lattice structures.

i Biocompatibility: *In vitro* biocompatibility of AM biodegradable porous metals is mainly determined by the released ion concentration. As porous metals generally degrade faster than bulk materials, the current cytotoxicity testing standard is not appropriate for AM biodegradable porous metals. AM porous magnesium and zinc showed better biocompatibility than AM porous iron *in vitro*. The cytotoxicity of AM Fe-based materials needs to be systematically studied *in vitro*, as the results available from the different studies published to date are contradictory.

That may require more consistent methodologies such as those used in Round-robin tests. The influence of the geometrical design of AM biodegradable porous metals on the cell responses should be systematically investigated using both experimental and numerical approaches. Functional coatings can be applied to improve both the biodegradation resistance and biocompatibility of AM porous biodegradable metals. Better surface polishing methods and exquisite surface patterning procedures need to be developed for AM biodegradable porous metals.

ii Bone formation: AM biodegradable porous metals can be bioactive materials in the human body once implanted, which can influence the bone tissue regeneration process through both biophysical and biochemical properties. AM porous magnesium and zinc are considered more appropriate than AM porous iron for orthopedic applications. Since there is still a large gap between the *in vitro* and *in vivo* results that are available for biodegradable metals, *in vivo* tests are required to evaluate the performance of AM biodegradable porous metals in actual service conditions.

Statement of significance

Additively manufactured (AM) biodegradable porous metals provide unprecedented opportunities for fulfilling the requirements of an ideal bone implant. Unlike several papers reviewing the AM of biodegradable metals mainly from the materials processing viewpoint, this review paper presents the state of the art in AM biodegradable porous metals and is focused on the effects of material type, processing, geometrical design, and post-AM treatments on the mechanical properties, biodegradation behavior, *in vitro* biocompatibility, and *in vivo* bone regeneration performance of AM porous Mg, Fe, and Zn as well as their alloys. We also identify a number of knowledge gaps and the challenges encountered in adopting AM biodegradable porous metals for orthopedic applications and suggest some promising areas for future research.

Declaration of Competing Interest

The authors declare that they have no known competing financial interests or personal relationships that could have appeared to influence the work reported in this paper.

References

[1] M. Geetha, A.K. Singh, R. Asokamani, A.K. Gogia, Ti based biomaterials, the ultimate choice for orthopaedic implants – A review, Prog Mater Sci 54 (2009) 397–425.
[2] D. Zhao, F. Witte, F. Lu, J. Wang, J. Li, L. Qin, Current status on clinical applications of magnesium-based orthopaedic implants: a review from clinical translational perspective, Biomaterials 112 (2017) 287–302.
[3] S. Wu, X. Liu, K.W.K. Yeung, C. Liu, X. Yang, Biomimetic porous scaffolds for bone tissue engineering, Mater Sci Eng R Rep 80 (2014) 1–36.
[4] L. Zhang, G. Yang, B.N. Johnson, X. Jia, Three-dimensional (3D) printed scaffold and material selection for bone repair, Acta Biomater 84 (2019) 16–33.
[5] R. Dimitriou, E. Jones, D. McGonagle, P.V. Giannoudis, Bone regeneration: current concepts and future directions, BMC Med 9 (2011) 66.
[6] W. Wang, K.W.K. Yeung, Bone grafts and biomaterials substitutes for bone defect repair: a review, Bioact Mater 2 (2017) 224–247.
[7] I.-.H. Oh, N. Nomura, N. Masahashi, S. Hanada, Mechanical properties of porous titanium compacts prepared by powder sintering, Scripta Mater 49 (2003) 1197–1202.
[8] C.E. Wen, M. Mabuchi, Y. Yamada, K. Shimojima, Y. Chino, T. Asahina, Processing of biocompatible porous Ti and Mg, Scripta Mater 45 (2001) 1147–1153.
[9] A.A. Zadpoor, Bone tissue regeneration: the role of scaffold geometry, Biomater Sci 3 (2015) 231–245.
[10] Y. Chen, Z. Xu, C. Smith, J. Sankar, Recent advances on the development of magnesium alloys for biodegradable implants, Acta Biomater 10 (2014) 4561–4573.
[11] A. Oryan, S. Alidadi, A. Moshiri, N. Maffulli, Bone regenerative medicine: classic options, novel strategies, and future directions, J Orthop Surg Res 9 (2014) 18.
[12] A.-.V. Do, B. Khorsand, S.M. Geary, A.K. Salem, 3D printing of scaffolds for tissue regeneration applications, Adv Healthc Mater 4 (2015) 1742–1762.
[13] X. Liu, P.X. Ma, Polymeric scaffolds for bone tissue engineering, Ann Biomed Eng 32 (2004) 477–486.
[14] H. Seitz, W. Rieder, S. Irsen, B. Leukers, C. Tille, Three-dimensional printing of porous ceramic scaffolds for bone tissue engineering, J Biomed Mater Res B Appl Biomater 74B (2005) 782–788.
[15] Q. Chen, G.A. Thouas, Metallic implant biomaterials, Mater Sci Eng R Rep 87 (2015) 1–57.
[16] I.A. van Hengel, M. Riool, L.E. Fratila-Apachitei, J. Witte-Bouma, E. Farrell, A.A. Zadpoor, S.A. Zaat, I. Apachitei, Selective laser melting porous metallic implants with immobilized silver nanoparticles kill and prevent biofilm formation by methicillin-resistant Staphylococcus aureus, Biomaterials (2017).
[17] M. Moravej, D. Mantovani, Biodegradable metals for cardiovascular stent application: interests and new opportunities, Int J Mol Sci 12 (2011) 4250.
[18] H. Hermawan, Updates on the research and development of absorbable metals for biomedical applications, Prog Biomater 7 (2018) 93–110.
[19] X. Wang, S. Xu, S. Zhou, W. Xu, M. Leary, P. Choong, M. Qian, M. Brandt, Y.M. Xie, Topological design and additive manufacturing of porous metals for bone scaffolds and orthopaedic implants: a review, Biomaterials 83 (2016) 127–141.
[20] A.A. Zadpoor, Mechanical performance of additively manufactured meta-biomaterials, Acta Biomater 85 (2019) 41–59.
[21] S.J.P. Callens, R.J.C. Uyttendaele, L.E. Fratila-Apachitei, A.A. Zadpoor, Substrate curvature as a cue to guide spatiotemporal cell and tissue organization, Biomaterials 232 (2020) 119739.
[22] Y. Xie, L. Zhao, Z. Zhang, X. Wang, R. Wang, C. Cui, Fabrication and properties of porous Zn-Ag alloy scaffolds as biodegradable materials, Mater Chem Phys 219 (2018) 433–443.
[23] L. Zhao, Z. Zhang, Y. Song, S. Liu, Y. Qi, X. Wang, Q. Wang, C. Cui, Mechanical properties and *in vitro* biodegradation of newly developed porous Zn scaffolds for biomedical applications, Mater Des 108 (2016) 136–144.
[24] R. Alavi, A. Trenggono, S. Champagne, H. Hermawan, Investigation on mechanical behavior of biodegradable iron foams under different compression test conditions, Metals (Basel) 7 (2017) 202.
[25] M. Heiden, E. Nauman, L. Stanciu, Bioresorbable Fe-Mn and Fe-Mn-HA materials for orthopedic implantation: enhancing degradation through porosity control, Adv Healthc Mater 6 (2017).
[26] K. Bobe, E. Willbold, I. Morgenthal, O. Andersen, T. Studnitzky, J. Nellesen, W. Tillmann, C. Vogt, K. Vano, F. Witte, *In vitro* and *in vivo* evaluation of biodegradable, open-porous scaffolds made of sintered magnesium W4 short fibres, Acta Biomater 9 (2013) 8611–8623.
[27] M.-q. Cheng, T. Wahafu, G.-f. Jiang, W. Liu, Y.-q. Qiao, X.-c. Peng, T. Cheng, X.-l. Zhang, G. He, X.-y. Liu, A novel open-porous magnesium scaffold with controllable microstructures and properties for bone regeneration, Sci Rep. 6 (2016) 24134.
[28] G. Jiang, G. He, A new approach to the fabrication of porous magnesium with well-controlled 3D pore structure for orthopedic applications, Mater Sci Eng, C. 43 (2014) 317–320.
[29] Z. Chen, X. Mao, L. Tan, T. Friis, C. Wu, R. Crawford, Y. Xiao, Osteoimmunomodulatory properties of magnesium scaffolds coated with β-tricalcium phosphate, Biomaterials 35 (2014) 8553–8565.
[30] X.N. Gu, W.R. Zhou, Y.F. Zheng, Y. Liu, Y.X. Li, Degradation and cytotoxicity of lotus-type porous pure magnesium as potential tissue engineering scaffold material, Mater Lett 64 (2010) 1871–1874.
[31] M.-.H. Kang, H.-.D. Jung, S.-.W. Kim, S.-.M. Lee, H.-.E. Kim, Y. Estrin, Y.-.H. Koh, Production and bio-corrosion resistance of porous magnesium with hydroxyapatite coating for biomedical applications, Mater Lett 108 (2013) 122–124.
[32] T. Lili, G. Mingming, Z. Feng, Z. Bingchun, Y. Ke, Study on compression behavior of porous magnesium used as bone tissue engineering scaffolds, Biomed Mater 4 (2009) 015016.
[33] Y.J. Liu, Z.Y. Yang, L.L. Tan, H. Li, Y.Z. Zhang, An animal experimental study of porous magnesium scaffold degradation and osteogenesis, Braz J Med Biol Res 47 (2014) 715–720.
[34] A.P. Md Saad, R.A. Abdul Rahim, M.N. Harun, H. Basri, J. Abdullah, M.R. Abdul Kadir, A. Syahrom, The influence of flow rates on the dynamic degradation behaviour of porous magnesium under a simulated environment of human cancellous bone, Mater Des 122 (2017) 268–279.
[35] A.P. Md Saad, A. Syahrom, Study of dynamic degradation behaviour of porous magnesium under physiological environment of human cancellous bone, Corros Sci 131 (2018) 45–56.
[36] A.P. Md. Saad, N. Jasmawati, M.N. Harun, M.R. Abdul Kadir, H. Nur, H. Hermawan, A. Syahrom, Dynamic degradation of porous magnesium under a simulated environment of human cancellous bone, Corros Sci 112 (2016) 495–506.
[37] S. Meininger, S. Mandal, A. Kumar, J. Groll, B. Basu, U. Gbureck, Strength reliability and *in vitro* degradation of three-dimensional powder printed strontium-substituted magnesium phosphate scaffolds, Acta Biomater 31 (2016) 401–411.
[38] I. Morgenthal, O. Andersen, C. Kostmann, G. Stephani, T. Studnitzky, F. Witte, B. Kieback, Highly porous magnesium alloy structures and their properties regarding degradable implant application, Adv Eng Mater 16 (2014) 309–318.
[39] M.P. Staiger, A.M. Pietak, J. Huadmai, G. Dias, Magnesium and its alloys as orthopedic biomaterials: a review, Biomaterials 27 (2006) 1728–1734.
[40] L. Tan, M. Gong, F. Zheng, B. Zhang, K. Yang, Study on compression behavior of porous magnesium used as bone tissue engineering scaffolds, Biomed Mater 4 (2009) 015016.

[41] W. Wang, G. Jia, Q. Wang, H. Huang, X. Li, H. Zeng, W. Ding, F. Witte, C. Zhang, W. Jia, G. Yuan, The *in vitro* and *in vivo* biological effects and osteogenic activity of novel biodegradable porous Mg alloy scaffolds, Mater Des 189 (2020) 108514.
[42] C.E. Wen, Y. Yamada, K. Shimojima, Y. Chino, H. Hosokawa, M. Mabuchi, Compressibility of porous magnesium foam: dependency on porosity and pore size, Mater Lett 58 (2004) 357–360.
[43] F. Witte, H. Ulrich, C. Palm, E. Willbold, Biodegradable magnesium scaffolds: part II: peri-implant bone remodeling, J Biomed Mater Res A 81 (2007) 757–765.
[44] F. Witte, H. Ulrich, M. Rudert, E. Willbold, Biodegradable magnesium scaffolds: part 1: appropriate inflammatory response, J Biomed Mater Res A 81 (2007) 748–756.
[45] M. Yazdimamaghani, M. Razavi, D. Vashaee, L. Tayebi, Development and degradation behavior of magnesium scaffolds coated with polycaprolactone for bone tissue engineering, Mater Lett 132 (2014) 106–110.
[46] W. Yu, H. Zhao, Z. Ding, Z. Zhang, B. Sun, J. Shen, S. Chen, B. Zhang, K. Yang, M. Liu, D. Chen, Y. He, *In vitro* and *in vivo* evaluation of MgF2 coated AZ31 magnesium alloy porous scaffolds for bone regeneration, Colloids Surf B 149 (2017) 330–340.
[47] L. Yuan, L. Yanxiang, W. Jiang, Z. Huawei, Evaluation of porosity in lotus-type porous magnesium fabricated by metal/gas eutectic unidirectional solidification, Mater Sci Eng C 402 (2005) 47–54.
[48] X. Zhang, X.-.W. Li, J.-.G. Li, X.-.D. Sun, Preparation and mechanical property of a novel 3D porous magnesium scaffold for bone tissue engineering, Mater Sci Eng C 42 (2014) 362–367.
[49] H. Zhuang, Y. Han, A. Feng, Preparation, mechanical properties and *in vitro* biodegradation of porous magnesium scaffolds, Mater Sci Eng C 28 (2008) 1462–1466.
[50] M.-.H. Kang, H. Lee, T.-.S. Jang, Y.-.J. Seong, H.-.E. Kim, Y.-.H. Koh, J. Song, H.-.D. Jung, Biomimetic porous Mg with tunable mechanical properties and biodegradation rates for bone regeneration, Acta Biomater 84 (2019) 453–467.
[51] L. Haverová, R. Oriňaková, A. Oriňak, R. Gorejová, M. Baláž, P. Vanýsek, M. Kupková, M. Hrubovčáková, P. Mudroň, J. Radoňák, Z. Orságová Králová, A. Morovská Turoňová, An *in vitro* corrosion study of open cell iron structures with PEG coating for bone replacement applications, Metals (Basel) 8 (2018) 499.
[52] N. Mohd Daud, N.B. Sing, A.H. Yusop, F.A. Abdul Majid, H. Hermawan, Degradation and *in vitro* cell–material interaction studies on hydroxyapatite-coated biodegradable porous iron for hard tissue scaffolds, J Orthop Translat 2 (2014) 177–184.
[53] Y. Qi, H. Qi, Y. He, W. Lin, P. Li, L. Qin, Y. Hu, L. Chen, Q. Liu, H. Sun, Q. Liu, G. Zhang, S. Cui, J. Hu, L. Yu, D. Zhang, J. Ding, Strategy of metal–polymer composite stent to accelerate biodegradation of iron-based biomaterials, ACS Appl Mater Interfaces 10 (2018) 182–192.
[54] Y. Su, S. Champagne, A. Trenggono, R. Tolouei, D. Mantovani, H. Hermawan, Development and characterization of silver containing calcium phosphate coatings on pure iron foam intended for bone scaffold applications, Mater Des 148 (2018) 124–134.
[55] A.H.M. Yusop, N.M. Daud, H. Nur, M.R.A. Kadir, H. Hermawan, Controlling the degradation kinetics of porous iron by poly (lactic-co-glycolic acid) infiltration for use as temporary medical implants, Sci Rep 5 (2015).
[56] Y. Hou, G. Jia, R. Yue, C. Chen, J. Pei, H. Zhang, H. Huang, M. Xiong, G. Yuan, Synthesis of biodegradable Zn-based scaffolds using NaCl templates: relationship between porosity, compressive properties and degradation behavior, Mater Charact 137 (2018) 162–169.
[57] Y. Qin, P. Wen, H. Guo, D. Xia, Y. Zheng, L. Jauer, R. Poprawe, M. Voshage, J.H. Schleifenbaum, Additive manufacturing of biodegradable metals: current research status and future perspectives, Acta Biomater (2019).
[58] T. DebRoy, H.L. Wei, J.S. Zuback, T. Mukherjee, J.W. Elmer, J.O. Milewski, A.M. Beese, A. Wilson-Heid, A. De, W. Zhang, Additive manufacturing of metallic components – Process, structure and properties, Prog Mater Sci 92 (2018) 112–224.
[59] R. Wauthle, S.M. Ahmadi, S. Amin Yavari, M. Mulier, A.A. Zadpoor, H. Weinans, J. Van Humbeeck, J.-.P. Kruth, J. Schrooten, Revival of pure titanium for dynamically loaded porous implants using additive manufacturing, Mater Sci Eng, C. 54 (2015) 94–100.
[60] J. Van der Stok, O.P. Van der Jagt, S. Amin Yavari, M.F.P. De Haas, J.H. Waarsing, H. Jahr, E.M.M. Van Lieshout, P. Patka, J.A.N. Verhaar, A.A. Zadpoor, H. Weinans, Selective laser melting-produced porous titanium scaffolds regenerate bone in critical size cortical bone defects, J Orthop Res 31 (2013) 792–799.
[61] S. Ahmadi, S. Yavari, R. Wauthle, B. Pouran, J. Schrooten, H. Weinans, A. Zadpoor, Additively manufactured open-cell porous biomaterials made from six different space-filling unit cells: the mechanical and morphological properties, Materials (Basel) 8 (2015) 1871.
[62] F. Bobbert, K. Lietaert, A. Eftekhari, B. Pouran, S. Ahmadi, H. Weinans, A. Zadpoor, Additively manufactured metallic porous biomaterials based on minimal surfaces: a unique combination of topological, mechanical, and mass transport properties, Acta Biomater 53 (2017) 572–584.
[63] C. Yan, L. Hao, A. Hussein, P. Young, D. Raymont, Advanced lightweight 316L stainless steel cellular lattice structures fabricated via selective laser melting, Mater Des 55 (2014) 533–541.
[64] R. Wauthle, J. van der Stok, S. Amin Yavari, J. Van Humbeeck, J.-.P. Kruth, A.A. Zadpoor, H. Weinans, M. Mulier, J. Schrooten, Additively manufactured porous tantalum implants, Acta Biomater 14 (2015) 217–225.
[65] S. Limmahakhun, A. Oloyede, K. Sitthiseripratip, Y. Xiao, C. Yan, Stiffness and strength tailoring of cobalt chromium graded cellular structures for stress-shielding reduction, Mater Des 114 (2017) 633–641.
[66] J.P. Kruth, L. Froyen, J. Van Vaerenbergh, P. Mercelis, M. Rombouts, B. Lauwers, Selective laser melting of iron-based powder, J Mater Process Technol 149 (2004) 616–622.
[67] Y. Qin, P. Wen, H. Guo, D. Xia, Y. Zheng, L. Jauer, R. Poprawe, M. Voshage, J.H. Schleifenbaum, Additive manufacturing of biodegradable metals: current research status and future perspectives, Acta Biomater 98 (2019) 3–22.
[68] R. Karunakaran, S. Ortgies, A. Tamayol, F. Bobaru, M.P. Sealy, Additive manufacturing of magnesium alloys, Bioact Mater 5 (2020) 44–54.
[69] Y.F. Zheng, X.N. Gu, F. Witte, Biodegradable metals, Mater Sci Eng R Rep 77 (2014) 1–34.
[70] D. Bian, W. Zhou, Y. Liu, N. Li, Y. Zheng, Z. Sun, Fatigue behaviors of HP-Mg, Mg–Ca and Mg–Zn–Ca biodegradable metals in air and simulated body fluid, Acta Biomater. 41 (2016) 351–360.
[71] B. Song, S. Dong, Q. Liu, H. Liao, C. Coddet, Vacuum heat treatment of iron parts produced by selective laser melting: microstructure, residual stress and tensile behavior, Mater Des 54 (2014) 727–733.
[72] B. Song, S. Dong, S. Deng, H. Liao, C. Coddet, Microstructure and tensile properties of iron parts fabricated by selective laser melting, Opt Laser Technol 56 (2014) 451–460.
[73] M. Montani, A.G. Demir, E. Mostaed, M. Vedani, B. Previtali, Processability of pure Zn and pure Fe by SLM for biodegradable metallic implant manufacturing, Rapid Prototyp J 23 (2017) 514–523.
[74] C.C. Ng, M.M. Savalani, M.L. Lau, H.C. Man, Microstructure and mechanical properties of selective laser melted magnesium, Appl Surf Sci 257 (2011) 7447–7454.
[75] C.C. Ng, M. Savalani, H.C. Man, Fabrication of magnesium using selective laser melting technique, Rapid Prototyp J 17 (2011) 479–490.
[76] Y. Zhou, P. Wu, Y. Yang, D. Gao, P. Feng, C. Gao, H. Wu, Y. Liu, H. Bian, C. Shuai, The microstructure, mechanical properties and degradation behavior of laser-melted MgSn alloys, J Alloys Compd 687 (2016) 109–114.
[77] M. Krystýnová, P. Doležal, S. Fintová, M. Březina, J. Zapletal, J. Wasserbauer, Preparation and characterization of zinc materials prepared by powder metallurgy, Metals (Basel) 7 (2017) 396.
[78] P. Wen, M. Voshage, L. Jauer, Y. Chen, Y. Qin, R. Poprawe, J.H. Schleifenbaum, Laser additive manufacturing of Zn metal parts for biodegradable applications: processing, formation quality and mechanical properties, Mater Des 155 (2018) 36–45.
[79] Y. Yang, F. Yuan, C. Gao, P. Feng, L. Xue, S. He, C. Shuai, A combined strategy to enhance the properties of Zn by laser rapid solidification and laser alloying, J Mech Behav Biomed Mater 82 (2018) 51–60.
[80] C. Shuai, L. Xue, C. Gao, Y. Yang, S. Peng, Y. Zhang, Selective laser melting of Zn–Ag alloys for bone repair: microstructure, mechanical properties and degradation behaviour, Virtual Phys Prototyp 13 (2018) 146–154.
[81] N.A. Zumdick, L. Jauer, L.C. Kersting, T.N. Kutz, J.H. Schleifenbaum, D. Zander, Additive manufactured WE43 magnesium: a comparative study of the microstructure and mechanical properties with those of powder extruded and as-cast WE43, Mater Charact 147 (2019) 384–397.
[82] P.K. Bowen, J.-.M. Seitz, R.J. Guillory II, J.P. Braykovich, S. Zhao, J. Goldman, J.W. Drelich, Evaluation of wrought Zn–Al alloys (1, 3, and 5 wt% Al) through mechanical and *in vivo* testing for stent applications, J Biomed Mater Res B 106 (2018) 245–258.
[83] H. Yang, B. Jia, Z. Zhang, X. Qu, G. Li, W. Lin, D. Zhu, K. Dai, Y. Zheng, Alloying design of biodegradable zinc as promising bone implants for load-bearing applications, Nat Commun 11 (2020) 401.
[84] D. Carluccio, C. Xu, J. Venezuela, Y. Cao, D. Kent, M. Bermingham, A.G. Demir, B. Previtali, Q. Ye, M. Dargusch, Additively manufactured iron-manganese for biodegradable porous load-bearing bone scaffold applications, Acta Biomater 103 (2020) 346–360.
[85] C. Shuai, W. Yang, Y. Yang, H. Pan, C. He, F. Qi, D. Xie, H. Liang, Selective laser melted Fe-Mn bone scaffold: microstructure, corrosion behavior and cell response, Mater Res Express 7 (2020) 015404.
[86] Y. Li, H. Jahr, X.Y. Zhang, M.A. Leeflang, W. Li, B. Pouran, F.D. Tichelaar, H. Weinans, J. Zhou, A.A. Zadpoor, Biodegradation-affected fatigue behavior of additively manufactured porous magnesium, Addit Manuf 28 (2019) 299–311.
[87] Y. Li, W. Li, F.S.L. Bobbert, K. Lietaert, J.H. Dong, M.A. Leeflang, J. Zhou, A.A. Zadpoor, Corrosion fatigue behavior of additively manufactured biodegradable porous zinc, Acta Biomater (2020).
[88] Y. Li, K. Lietaert, W. Li, X.Y. Zhang, M.A. Leeflang, J. Zhou, A.A. Zadpoor, Corrosion fatigue behavior of additively manufactured biodegradable porous iron, Corros Sci 156 (2019) 106–116.
[89] S.M. Ahmadi, R. Hedayati, Y. Li, K. Lietaert, N. Tümer, A. Fatemi, C.D. Rans, B. Pouran, H. Weinans, A.A. Zadpoor, Fatigue performance of additively manufactured meta-biomaterials: the effects of topology and material type, Acta Biomater 65 (2018) 292–304.
[90] K. Wei, M. Gao, Z. Wang, X. Zeng, Effect of energy input on formability, microstructure and mechanical properties of selective laser melted AZ91D magnesium alloy, Mater Sci Eng C 611 (2014) 212–222.
[91] V. Manakari, G. Parande, M. Gupta, Selective laser melting of magnesium and magnesium alloy powders: a review, Metals (Basel) 7 (2016) 2.
[92] Y. Qin, P. Wen, D. Xia, H. Guo, M. Voshage, L. Jauer, Y. Zheng, J.H. Schleifenbaum, Y. Tian, Effect of grain structure on the mechanical properties and *in vitro* corrosion behavior of additively manufactured pure Zn, Addit Manuf (2020) 101134.

[93] Y. Li, H. Jahr, K. Lietaert, P. Pavanram, A. Yilmaz, L.I. Fockaert, M.A. Leeflang, B. Pouran, Y. Gonzalez-Garcia, H. Weinans, J.M.C. Mol, J. Zhou, A.A. Zadpoor, Additively manufactured biodegradable porous iron, Acta Biomater 77 (2018) 380–393.

[94] Y. Li, P. Pavanram, J. Zhou, K. Lietaert, P. Taheri, W. Li, H. San, M.A. Leeflang, J.M.C. Mol, H. Jahr, A.A. Zadpoor, Additively manufactured biodegradable porous zinc, Acta Biomater 101 (2020) 609–623.

[95] Y. Li, J. Zhou, P. Pavanram, M.A. Leeflang, L.I. Fockaert, B. Pouran, N. Tümer, K.U. Schröder, J.M.C. Mol, H. Weinans, H. Jahr, A.A. Zadpoor, Additively manufactured biodegradable porous magnesium, Acta Biomater 67 (2018) 378–392.

[96] D.-.T. Chou, D. Wells, D. Hong, B. Lee, H. Kuhn, P.N. Kumta, Novel processing of iron–manganese alloy-based biomaterials by inkjet 3-D printing, Acta Biomater 9 (2013) 8593–8603.

[97] D. Hong, D.-.T. Chou, O.I. Velikokhatnyi, A. Roy, B. Lee, I. Swink, I. Issaev, H.A. Kuhn, P.N. Kumta, Binder-jetting 3D printing and alloy development of new biodegradable Fe-Mn-Ca/Mg alloys, Acta Biomater 45 (2016) 375–386.

[98] P. Sharma, K.G. Jain, P.M. Pandey, S. Mohanty, *In vitro* degradation behaviour, cytocompatibility and hemocompatibility of topologically ordered porous iron scaffold prepared using 3D printing and pressureless microwave sintering, Mater Sci Eng C 106 (2020) 110247.

[99] Y. Li, H. Jahr, P. Pavanram, F.S.L. Bobbert, U. Puggi, X.Y. Zhang, B. Pouran, M.A. Leeflang, H. Weinans, J. Zhou, A.A. Zadpoor, Additively manufactured functionally graded biodegradable porous iron, Acta Biomater 96 (2019) 646–661.

[100] Y. Li, P. Pavanram, J. Zhou, K. Lietaert, F.S.L. Bobbert, Y. Kubo, M.A. Leeflang, H. Jahr, A.A. Zadpoor, Additively manufactured functionally graded biodegradable porous zinc, Biomater Sci (2020).

[101] A.A. Zadpoor, Additively manufactured porous metallic biomaterials, J Mater Chem B 7 (2019) 4088–4117.

[102] V.S. Deshpande, M.F. Ashby, N.A. Fleck, Foam topology: bending *versus* stretching dominated architectures, Acta Mater 49 (2001) 1035–1040.

[103] K. Lietaert, A.A. Zadpoor, M. Sonnaert, J. Schrooten, L. Weber, A. Mortensen, J. Vleugels, Mechanical properties and cytocompatibility of dense and porous Zn produced by laser powder bed fusion for biodegradable implant applications, Acta Biomater (2020).

[104] R. Wauthle, B. Vrancken, B. Beynaerts, K. Jorissen, J. Schrooten, J.-.P. Kruth, J. Van Humbeeck, Effects of build orientation and heat treatment on the microstructure and mechanical properties of selective laser melted Ti6Al4V lattice structures, Addit Manuf 5 (2015) 77–84.

[105] M. Mazur, M. Leary, S. Sun, M. Vcelka, D. Shidid, M. Brandt, Deformation and failure behaviour of Ti-6Al-4V lattice structures manufactured by selective laser melting (SLM), Int J Adv Manuf Technol 84 (2016) 1391–1411.

[106] A.A. Zadpoor, G. Campoli, H. Weinans, Neural network prediction of load from the morphology of trabecular bone, Appl Math Model 37 (2013) 5260–5276.

[107] J. Hazrati Marangalou, K. Ito, B. van Rietbergen, A novel approach to estimate trabecular bone anisotropy from stress tensors, Biomech Model Mechanobiol 14 (2015) 39–48.

[108] D.M. Geraldes, A.T.M. Phillips, A comparative study of orthotropic and isotropic bone adaptation in the femur, Int J Numer Method Biomed Eng 30 (2014) 873–889.

[109] P. Christen, K. Ito, I. Knippels, R. Müller, G.H. van Lenthe, B. van Rietbergen, Subject-specific bone loading estimation in the human distal radius, J Biomech 46 (2013) 759–766.

[110] G. Campoli, H. Weinans, A.A. Zadpoor, Computational load estimation of the femur, J Mech Behav Biomed Mater 10 (2012) 108–119.

[111] K. Nune, A. Kumar, R. Misra, S. Li, Y. Hao, R. Yang, Osteoblast functions in functionally graded Ti-6Al-4V mesh structures, J Biomater Appl 30 (2016) 1182–1204.

[112] X.-.Y. Zhang, G. Fang, S. Leeflang, A.A. Zadpoor, J. Zhou, Topological design, permeability and mechanical behavior of additively manufactured functionally graded porous metallic biomaterials, Acta Biomater 84 (2019) 437–452.

[113] S. Zhao, S.J. Li, S.G. Wang, W.T. Hou, Y. Li, L.C. Zhang, Y.L. Hao, R. Yang, R.D.K. Misra, L.E. Murr, Compressive and fatigue behavior of functionally graded Ti-6Al-4V meshes fabricated by electron beam melting, Acta Mater 150 (2018) 1–15.

[114] P. Wen, L. Jauer, M. Voshage, Y. Chen, R. Poprawe, J.H. Schleifenbaum, Densification behavior of pure Zn metal parts produced by selective laser melting for manufacturing biodegradable implants, J Mater Process Technol 258 (2018) 128–137.

[115] S.M. Ahmadi, R. Kumar, E.V. Borisov, R. Petrov, S. Leeflang, Y. Li, N. Tümer, R. Huizenga, C. Ayas, A.A. Zadpoor, V.A. Popovich, From microstructural design to surface engineering: a tailored approach for improving fatigue life of additively manufactured meta-biomaterials, Acta Biomater 83 (2019) 153–166.

[116] A. Kopp, T. Derra, M. Müther, L. Jauer, J.H. Schleifenbaum, M. Voshage, O. Jung, R. Smeets, N. Kröger, Influence of design and postprocessing parameters on the degradation behavior and mechanical properties of additively manufactured magnesium scaffolds, Acta Biomater 98 (2019) 23–35.

[117] M.-.W. Wu, J.-.K. Chen, B.-.H. Lin, P.-.H. Chiang, Improved fatigue endurance ratio of additive manufactured Ti-6Al-4V lattice by hot isostatic pressing, Mater Des 134 (2017) 163–170.

[118] C. Yang, Z. Huan, X. Wang, C. Wu, J. Chang, 3D printed Fe scaffolds with HA nanocoating for bone regeneration, ACS Biomater Sci Eng 4 (2018) 608–616.

[119] B. Yuan, G.M. Guss, A.C. Wilson, S.P. Hau-Riege, P.J. DePond, S. McMains, M.J. Matthews, B. Giera, Machine-learning-based monitoring of laser powder bed fusion, Adv Mater Technol 3 (2018) 1800136.

[120] B. Kappes, S. Moorthy, D. Drake, H. Geerlings, A. Stebner, in: Machine learning to optimize additive manufacturing parameters for laser powder bed fusion of inconel 718, Springer International Publishing, Cham, 2018, pp. 595–610.

[121] A. Caggiano, J. Zhang, V. Alfieri, F. Caiazzo, R. Gao, R. Teti, Machine learning-based image processing for on-line defect recognition in additive manufacturing, CIRP Annals 68 (2019) 451–454.

[122] J. Venezuela, M.S. Dargusch, The influence of alloying and fabrication techniques on the mechanical properties, biodegradability and biocompatibility of zinc: a comprehensive review, Acta Biomater 87 (2019) 1–40.

[123] C. Shuai, C. He, P. Feng, W. Guo, C. Gao, P. Wu, Y. Yang, S. Bin, Biodegradation mechanisms of selective laser-melted Mg–xAl–Zn alloy: grain size and intermetallic phase, Virtual Phys Prototyp 13 (2018) 59–69.

[124] K.D. Ralston, N. Birbilis, C.H.J. Davies, Revealing the relationship between grain size and corrosion rate of metals, Scripta Mater 63 (2010) 1201–1204.

[125] W.R. Osório, C.M. Freire, A. Garcia, The role of macrostructural morphology and grain size on the corrosion resistance of Zn and Al castings, Mater Sci Eng C 402 (2005) 22–32.

[126] K.M.S. Youssef, C.C. Koch, P.S. Fedkiw, Improved corrosion behavior of nanocrystalline zinc produced by pulse-current electrodeposition, Corros Sci 46 (2004) 51–64.

[127] R. Walter, M.B. Kannan, Y. He, A. Sandham, Effect of surface roughness on the *in vitro* degradation behaviour of a biodegradable magnesium-based alloy, Appl Surf Sci 279 (2013) 343–348.

[128] X.N. Gu, W.R. Zhou, Y.F. Zheng, Y. Cheng, S.C. Wei, S.P. Zhong, T.F. Xi, L.J. Chen, Corrosion fatigue behaviors of two biomedical Mg alloys – AZ91D and WE43 – In simulated body fluid, Acta Biomater 6 (2010) 4605–4613.

[129] J. Xie, A.T. Alpas, D.O. Northwood, A mechanism for the crack initiation of corrosion fatigue of Type 316L stainless steel in Hank's solution, Mater Charact 48 (2002) 271–277.

[130] J. Yang, Q. Wang, K. Guan, Effect of stress and strain on corrosion resistance of duplex stainless steel, Int J Press Vessel Pip 110 (2013) 72–76.

[131] G. LÜ, H. Cheng, C. Xu, Z. He, Effect of strain and chloride concentration on pitting susceptibility for type 304 austenitic stainless steel, Chin J Chem Eng 16 (2008) 314–319.

[132] B.T. Lu, Z.K. Chen, J.L. Luo, B.M. Patchett, Z.H. Xu, Pitting and stress corrosion cracking behavior in welded austenitic stainless steel, Electrochim Acta 50 (2005) 1391–1403.

[133] A.H.M. Sanchez, B.J.C. Luthringer, F. Feyerabend, R. Willumeit, Mg and Mg alloys: how comparable are *in vitro* and *in vivo* corrosion rates? A review, Acta Biomater 13 (2015) 16–31.

[134] Z. Pei, D. Zhang, Y. Zhi, T. Yang, L. Jin, D. Fu, X. Cheng, H.A. Terryn, J.M.C. Mol, X. Li, Towards understanding and prediction of atmospheric corrosion of an Fe/Cu corrosion sensor via machine learning, Corros Sci 170 (2020) 108697.

[135] W. Frank, J. Lucas, M. Wolfgang, K. Zienab, S. Kristin, S. Tanja, Open-porous biodegradable magnesium scaffolds produced by selective laser melting for individualized bone replacement, Front Bioeng BioTech 4 (2016).

[136] C. Shuai, Y. Cheng, Y. Yang, S. Peng, W. Yang, F. Qi, Laser additive manufacturing of Zn-2Al part for bone repair: formability, microstructure and properties, J Alloys Compd 798 (2019) 606–615.

[137] D. Carluccio, C. Xu, J. Venezuela, Y. Cao, D. Kent, M. Bermingham, A.G. Demir, B. Previtali, Q. Ye, M. Dargusch, Additively manufactured iron-manganese for biodegradable porous load-bearing bone scaffold applications, Acta Biomater (2019).

[138] C. Gao, M. Yao, S. Li, P. Feng, S. Peng, C. Shuai, Highly biodegradable and bioactive Fe-Pd-bredigite biocomposites prepared by selective laser melting, J Adv Res 20 (2019) 91–104.

[139] C. Shuai, L. Liu, M. Zhao, P. Feng, Y. Yang, W. Guo, C. Gao, F. Yuan, Microstructure, biodegradation, antibacterial and mechanical properties of ZK60-Cu alloys prepared by selective laser melting technique, J Mater Sci Technol 34 (2018) 1944–1952.

[140] D. Hong, D.-.T. Chou, O.I. Velikokhatnyi, A. Roy, B. Lee, I. Swink, I. Issaev, H.A. Kuhn, P.N. Kumta, Binder-jetting 3D printing and alloy development of new biodegradable Fe-Mn-Ca/Mg alloys, Acta Biomater 45 (2016) 375–386.

[141] S. Bagherifard, R. Ghelichi, A. Khademhosseini, M. Guagliano, Cell response to nanocrystallized metallic substrates obtained through severe plastic deformation, ACS Appl Mater Interfaces 6 (2014) 7963–7985.

[142] P. Saha, M. Roy, M.K. Datta, B. Lee, P.N. Kumta, Effects of grain refinement on the biocorrosion and *in vitro* bioactivity of magnesium, Mater Sci Eng C 57 (2015) 294–303.

[143] B.R. Sunil, A.A. Kumar, T.S. Sampath Kumar, U. Chakkingal, Role of biomineralization on the degradation of fine grained AZ31 magnesium alloy processed by groove pressing, Mater Sci Eng C 33 (2013) 1607–1615.

[144] F.L. Nie, Y.F. Zheng, S.C. Wei, C. Hu, G. Yang, In vitrocorrosion, cytotoxicity and hemocompatibility of bulk nanocrystalline pure iron, Biomed Mater 5 (2010) 065015.

[145] T.J. Webster, J.U. Ejiofor, Increased osteoblast adhesion on nanophase metals: ti, Ti6Al4V, and CoCrMo, Biomaterials 25 (2004) 4731–4739.

[146] X.P. Tan, Y.J. Tan, C.S.L. Chow, S.B. Tor, W.Y. Yeong, Metallic powder-bed based 3D printing of cellular scaffolds for orthopaedic implants: a state-of-the-art review on manufacturing, topological design, mechanical properties and biocompatibility, Mater Sci Eng C 76 (2017) 1328–1343.

[147] S. Van Bael, Y.C. Chai, S. Truscello, M. Moesen, G. Kerckhofs, H. Van Oosterwyck, J.P. Kruth, J. Schrooten, The effect of pore geometry on the *in vitro* biological behavior of human periosteum-derived cells seeded on selective laser-melted Ti6Al4V bone scaffolds, Acta Biomater 8 (2012) 2824–2834.

[148] M. Yazdimamaghani, M. Razavi, D. Vashaee, K. Moharamzadeh, A.R. Boccaccini, L. Tayebi, Porous magnesium-based scaffolds for tissue engineering, Mater Sci Eng, C. 71 (2017) 1253–1266.
[149] Y. Su, K. Wang, J. Gao, Y. Yang, Y.-X. Qin, Y. Zheng, D. Zhu, Enhanced cytocompatibility and antibacterial property of zinc phosphate coating on biodegradable zinc materials, Acta Biomater 98 (2019) 174–185.
[150] P. Habibovic, J.E. Barralet, Bioinorganics and biomaterials: bone repair, Acta Biomater 7 (2011) 3013–3026.
[151] Y. Lai, Y. Li, H. Cao, J. Long, X. Wang, L. Li, C. Li, Q. Jia, B. Teng, T. Tang, J. Peng, D. Eglin, M. Alini, D.W. Grijpma, G. Richards, L. Qin, Osteogenic magnesium incorporated into PLGA/TCP porous scaffold by 3D printing for repairing challenging bone defect, Biomaterials 197 (2019) 207–219.
[152] N. Kleer, S. Julmi, A.K. Gartzke, J. Augustin, F. Feichtner, A.C. Waselau, C. Klose, H.J. Maier, P. Wriggers, A. Meyer-Lindenberg, Comparison of degradation behaviour and osseointegration of the two magnesium scaffolds, LAE442 and La2, *in vivo*, Materialia 8 (2019) 100436.
[153] A. Kafri, S. Ovadia, G. Yosafovich-Doitch, E. Aghion, *In vivo* performances of pure Zn and Zn–Fe alloy as biodegradable implants, J Mater Sci Mater Med 29 (2018) 94.
[154] X. Wang, X. Shao, T. Dai, F. Xu, J.G. Zhou, G. Qu, L. Tian, B. Liu, Y. Liu, *In vivo* study of the efficacy, biosafety, and degradation of a zinc alloy osteosynthesis system, Acta Biomater 92 (2019) 351–361.
[155] D. Zhu, I. Cockerill, Y. Su, Z. Zhang, J. Fu, K.-.W. Lee, J. Ma, C. Okpokwasili, L. Tang, Y. Zheng, Y.-.X. Qin, Y. Wang, Mechanical strength, biodegradation, and *in vitro* and *in vivo* biocompatibility of Zn biomaterials, ACS Appl Mater Interfaces (2019).
[156] C. Xiao, L. Wang, Y. Ren, S. Sun, E. Zhang, C. Yan, Q. Liu, X. Sun, F. Shou, J. Duan, H. Wang, G. Qin, Indirectly extruded biodegradable Zn-0.05wt%Mg alloy with improved strength and ductility: *in vitro* and *in vivo* studies, J Mater Sci Technol 34 (2018) 1618–1627.
[157] H.F. Li, X.H. Xie, Y.F. Zheng, Y. Cong, F.Y. Zhou, K.J. Qiu, X. Wang, S.H. Chen, L. Huang, L. Tian, L. Qin, Development of biodegradable Zn-1X binary alloys with nutrient alloying elements Mg, Ca and Sr, Sci Rep. 5 (2015) 10719.
[158] A. Braem, A. Chaudhari, M. Vivan Cardoso, J. Schrooten, J. Duyck, J. Vleugels, Peri- and intra-implant bone response to microporous Ti coatings with surface modification, Acta Biomater 10 (2014) 986–995.
[159] F. Bai, Z. Wang, J. Lu, J. Liu, G. Chen, R. Lv, J. Wang, K. Lin, J. Zhang, X. Huang, The correlation between the internal structure and vascularization of controllable porous bioceramic materials in vivo: a quantitative study, Tissue Eng Part A 16 (2010) 3791–3803.
[160] N. Taniguchi, S. Fujibayashi, M. Takemoto, K. Sasaki, B. Otsuki, T. Nakamura, T. Matsushita, T. Kokubo, S. Matsuda, Effect of pore size on bone ingrowth into porous titanium implants fabricated by additive manufacturing: an *in vivo* experiment, Mater Sci Eng C 59 (2016) 690–701.
[161] S. Ray, U. Thormann, M. Eichelroth, M. Budak, C. Biehl, M. Rupp, U. Sommer, T. El Khassawna, F.I. Alagboso, M. Kampschulte, M. Rohnke, A. Henß, K. Peppler, V. Linke, P. Quadbeck, A. Voigt, F. Stenger, D. Karl, R. Schnettler, C. Heiss, K.S. Lips, V. Alt, Strontium and bisphosphonate coated iron foam scaffolds for osteoporotic fracture defect healing, Biomaterials 157 (2018) 1–16.
[162] H. Yang, X. Qu, W. Lin, C. Wang, D. Zhu, K. Dai, Y. Zheng, *In vitro* and *in vivo* studies on zinc-hydroxyapatite composites as novel biodegradable metal matrix composite for orthopedic applications, Acta Biomater 71 (2018) 200–214.
[163] T. Kraus, F. Moszner, S. Fischerauer, M. Fiedler, E. Martinelli, J. Eichler, F. Witte, E. Willbold, M. Schinhammer, M. Meischel, P.J. Uggowitzer, J.F. Löffler, A. Weinberg, Biodegradable Fe-based alloys for use in osteosynthesis: outcome of an *in vivo* study after 52weeks, Acta Biomater 10 (2014) 3346–3353.
[164] M.D. Cappellini, J. Comin-Colet, A. de Francisco, A. Dignass, W. Doehner, C.S. Lam, I.C. Macdougall, G. Rogler, C. Camaschella, R. Kadir, N.J. Kassebaum, D.R. Spahn, A.T. Taher, K.M. Musallam, o. b. o. t. I. C. Group, Iron deficiency across chronic inflammatory conditions: international expert opinion on definition, diagnosis, and management, Am J Hematol 92 (2017) 1068–1078.
[165] W. Lin, L. Qin, H. Qi, D. Zhang, G. Zhang, R. Gao, H. Qiu, Y. Xia, P. Cao, X. Wang, W. Zheng, Long-term *in vivo* corrosion behavior, biocompatibility and bioresorption mechanism of a bioresorbable nitrided iron scaffold, Acta Biomater 54 (2017) 454–468.
[166] A.K. Gaharwar, I. Singh, A. Khademhosseini, Engineered biomaterials for *in situ* tissue regeneration, Nature Reviews Materials (2020).
[167] A.J. Engler, S. Sen, H.L. Sweeney, D.E. Discher, Matrix elasticity directs stem cell lineage specification, Cell 126 (2006) 677–689.
[168] Y. Zhang, J. Xu, Y.C. Ruan, M.K. Yu, M. O'Laughlin, H. Wise, D. Chen, L. Tian, D. Shi, J. Wang, S. Chen, J.Q. Feng, D.H.K. Chow, X. Xie, L. Zheng, L. Huang, S. Huang, K. Leung, N. Lu, L. Zhao, H. Li, D. Zhao, X. Guo, K. Chan, F. Witte, H.C. Chan, Y. Zheng, L. Qin, Implant-derived magnesium induces local neuronal production of CGRP to improve bone-fracture healing in rats, Nat Med 22 (2016) 1160–1169.
[169] M. Salehi, S. Maleksaeedi, S.M.L. Nai, G.K. Meenashisundaram, M.H. Goh, M. Gupta, A paradigm shift towards compositionally zero-sum binderless 3D printing of magnesium alloys via capillary-mediated bridging, Acta Mater 165 (2019) 294–306.
[170] J. Wu, L. Wang, Selective laser melting manufactured CNTs/AZ31B composites: heat transfer and vaporized porosity evolution, J Mater Res 33 (2018) 2752–2762.
[171] T. Kurzynowski, A. Pawlak, E. Chlebus, in: Processing of Magnesium Alloy by Selective Laser Melting, Springer International Publishing, Cham, 2019, pp. 411–418.
[172] K. Wei, X. Zeng, Z. Wang, J. Deng, M. Liu, G. Huang, X. Yuan, Selective laser melting of Mg-Zn binary alloys: effects of Zn content on densification behavior, microstructure, and mechanical property, Mater Sci Eng C 756 (2019) 226–236.
[173] F. Witte, L. Jauer, W. Meiners, Z. Kronbach, K. Strohschein, T. Schmidt, Open–porous biodegradable magnesium scaffolds produced by selective laser melting for individualized bone replacement, Front Bioeng BioTech 4 (2016).
[174] M. Salehi, S. Maleksaeedi, M.A.B. Sapari, M.L.S. Nai, G.K. Meenashisundaram, M. Gupta, Additive manufacturing of magnesium–zinc–zirconium (ZK) alloys via capillary-mediated binderless three-dimensional printing, Mater Des 169 (2019) 107683.
[175] I. Cockerill, Y. Su, S. Sinha, Y.-.X. Qin, Y. Zheng, M.L. Young, D. Zhu, Porous zinc scaffolds for bone tissue engineering applications: a novel additive manufacturing and casting approach, Mater Sci Eng C (2020) 110738.
[176] P.K. Bowen, J. Drelich, J. Goldman, Zinc exhibits ideal physiological corrosion behavior for bioabsorbable stents, Adv Mater 25 (2013) 2577–2582.
[177] C. He, S. Bin, P. Wu, C. Gao, P. Feng, Y. Yang, L. Liu, Y. Zhou, M. Zhao, S. Yang, C. Shuai, Microstructure evolution and biodegradation behavior of laser rapid solidified Mg–Al–Zn alloy, Metals (Basel) 7 (2017) 105.
[178] D. Carluccio, M. Bermingham, D. Kent, A.G. Demir, B. Previtali, M.S. Dargusch, Comparative study of pure iron manufactured by selective laser melting, laser metal deposition, and casting processes, Adv Eng Mater 21 (2019) 1900049.